

Cosmological Constraint Precision of the Photometric and Spectroscopic Multi-probe Surveys of China Space Station Telescope (CSST)

Haitao Miao^{1,2}, Yan Gong^{1,2}★, Xuelei Chen^{3,4,5,6}, Zhiqi Huang^{7,8}, Xiao-Dong Li^{7,8}, Hu Zhan^{1,9}

¹key laboratory of space astronomy and technology, National Astronomical Observatories, Chinese Academy of Sciences, Beijing 100101, People's Republic of China

²Science Center for China Space Station Telescope, National Astronomical Observatories, Chinese Academy of Sciences, Beijing 100101, People's Republic of China

³Key Laboratory for Computational Astrophysics, National Astronomical Observatories, Chinese Academy of Sciences, 20A Datun Road, Beijing 100101, China

⁴University of Chinese Academy of Sciences, Beijing 100049, People's Republic of China

⁵Centre for High Energy Physics, Peking University, Beijing 100871, People's Republic of China

⁶Department of Physics, College of Sciences, Northeastern University, Shenyang 110819, China

⁷School of Physics and Astronomy, Sun Yat-sen University, 2 Daxue Road, Tangjia, Zhuhai, 519082, China

⁸CSST Science Center for the Guangdong-Hongkong-Macau Greater Bay Area, SYSU, China

⁹Kavli Institute for Astronomy and Astrophysics, Peking University, Beijing 100871, China

Accepted XXX. Received YYY; in original form ZZZ

ABSTRACT

As one of Stage IV space-based telescopes, China Space Station Telescope (CSST) can perform photometric and spectroscopic surveys simultaneously to efficiently explore the Universe in extreme precision. In this work, we investigate several powerful CSST cosmological probes, including cosmic shear, galaxy-galaxy lensing, photometric and spectroscopic galaxy clustering, and number counts of galaxy clusters, and study the capability of these probes by forecasting the results of joint constraints on the cosmological parameters. By referring to real observational results, we generate mock data and estimate the measured errors based on CSST observational and instrumental designs. To study the systematical effects on the results, we also consider a number of systematics in CSST photometric and spectroscopic surveys, such as the intrinsic alignment, shear calibration uncertainties, photometric redshift uncertainties, galaxy bias, non-linear effects, instrumental effects, etc. The Fisher matrix method is used to derive the constraint results from individual or joint surveys on the cosmological and systematical parameters. We find that the joint constraints by including all these CSST cosmological probes can significantly improve the results from current observations by one order of magnitude at least, which gives Ω_m and σ_8 < 1% accuracy, and w_0 and w_a < 5% and 20% accuracies, respectively. This indicates that the CSST photometric and spectroscopic multi-probe surveys could provide powerful tools to explore the Universe and greatly improve the studies of relevant cosmological problems.

Key words: cosmology: galaxy clustering, galaxy survey, large-scale structure, weak lensing, galaxy clusters

1 INTRODUCTION

Based on a variety of observations in the past two decades (Percival et al. 2010; Eisenstein et al. 2011; Komatsu et al. 2011; Beutler et al. 2011; Sievers et al. 2013; Hinshaw et al. 2013; Hou et al. 2014; Planck Collaboration et al. 2014), we have entered the era of precision cosmology, and established the standard cosmological model. Current observations indicate that the Universe is composed of about 70% dark energy and 25% dark matter. Dark energy provides a physical mechanism for cosmic acceleration, and it is characterized by its equation of state (EOS) w , which is defined by the ratio of pressure to energy density. When $w = -1$, dark energy becomes the cosmological constant, that is a key component of the standard Lambda cold dark matter (Λ CDM) model. The Λ CDM model is supported by most of current observations (e.g. Planck Collaboration et al. 2020; Alam

et al. 2021). Although some tensions or challenges are still existing, such as missing satellites, cusp/core, and Hubble tension (see e.g. Bullock & Boylan-Kolchin 2017; Verde et al. 2019; Di Valentino et al. 2021), the Λ CDM model has achieved tremendous success. However, the nature of dark energy and dark matter is still poorly understood. We still face great challenges of finding a fundamental physical explanation for dark energy and dark matter. Dynamical dark energy models have been studied extensively, where the EOS is usually time-dependent in these models. The most popular model is the Chevallier-Polarski-Linder parameterization (CPL, Chevallier & Polarski 2001; Linder 2003), which is a Taylor expansion around $a = 1$, $w = w_0 + w_a(1 - a)$. A number of cosmological observations can provide valuable information to explore the nature of dark energy and dark matter with high precision, such as the surveys related to the cosmic large scale structure (LSS).

Galaxies formation is mainly caused by the collapse of matter under the effect of gravity. The spatial distribution of galaxies in

★ E-mail: gongyan@bao.ac.cn

the Universe contains a lot of information about the formation and evolution of cosmic structures. Galaxy catalogs with spectroscopic redshift are used to probe the three-dimensional structure of the Universe. The galaxy two-point spatial correlation function or power spectrum (i.e. Fourier transformation of the two-point correlation function) is often adopted in the data analysis. It can provide tight constraints on cosmological parameters by using only Baryon Acoustic Oscillation (BAO) wiggles (Seo & Eisenstein 2007; Font-Ribera et al. 2014) or full shape of galaxy power spectrum (Wang et al. 2013; d’Amico et al. 2020; Ivanov et al. 2020; Brieden et al. 2021).

On the other hand, although photometric observations have a large redshift uncertainty, they can detect and measure a large number of galaxies than spectroscopic observations. We can extract accurate information from the galaxy two-point angular correlation function or angular power spectrum, which can improve the ability of constraining the cosmological parameters. The results from ongoing and near-future photometric surveys have been studied (e.g. Zhan & Knox 2006; Padmanabhan et al. 2007; Zhan et al. 2009; Abbott et al. 2022b; Rosell et al. 2022; Rodríguez-Monroy et al. 2022). It has been shown that weak lensing is a precise cosmological probe by measuring shear information of galaxy images (Zhan 2006; Albrecht et al. 2006; Kilbinger 2015; Hildebrandt et al. 2017; Troxel et al. 2018; Amon et al. 2022). When the cross-correlation of the galaxy number density and galaxy shear is considered, more useful information and stringent constraint results can be obtained (Zhang et al. 2010; Benjamin et al. 2010; McQuinn & White 2013; Prat et al. 2018; Schaan et al. 2020; Prat et al. 2022). Hence, a joint analysis of weak lensing, galaxy clustering and galaxy-galaxy lensing (the so-called 3×2 pt probes) have been suggested and applied to observational data (e.g. Bernstein 2009; Joachimi & Bridle 2010; van Uitert et al. 2018; Krause et al. 2017; Krause & Eifler 2017; Eifler et al. 2021a; Euclid Collaboration et al. 2020; Joachimi et al. 2021; Krause et al. 2021). The results from Kilo-Degree Survey¹ (KiDS, Hildebrandt et al. 2017; Heymans et al. 2021; Tröster et al. 2021), Dark Energy Survey² (DES, Abbott et al. 2018; Krause et al. 2021; To et al. 2021a; Abbott et al. 2022a), and Hyper Suprime-Cam³ (HSC, Hikage et al. 2019) have demonstrated the approach of increasing the overall constraining power by jointly analyzing different cosmological probes.

Besides, number counts of galaxy clusters is also a powerful cosmological probe (e.g., Yoo & Seljak 2012; To et al. 2021b; Eifler et al. 2021b). Galaxy clusters are formed at high peak of the primary matter density field. The abundance of galaxy clusters is sensitive to the growth history of structures and the expansion history of the Universe. So the number counts of galaxy clusters have a strong dependence on several cosmological parameters, especially the amplitude parameter of the matter power spectrum σ_8 and the matter energy density parameter of the Universe Ω_m . The cluster number density evolving with redshift can break the degeneracy between these two parameters, and thus can be used to further constrain the cold dark matter and dark energy density parameters (Haiman et al. 2001; Lima & Hu 2005; Allen et al. 2011). Clusters can be identified and measured by using cluster richness and weak lensing in photometric and spectroscopic surveys (Rozo et al. 2010; Oguri & Takada 2011; Oguri 2014; Rozo et al. 2015; Rykoff et al. 2014; Simet et al. 2017). The cluster catalog constructed from optical wavelengths and applied to constraining the cosmological parameters have been extensively studied recently (e.g. de Haan et al. 2016; Sartoris et al.

2016; Heneka et al. 2018; Salvati et al. 2020; Fumagalli et al. 2021; Costanzi et al. 2019, 2021; Abdullah et al. 2020; Sunayama et al. 2020; Park et al. 2021a).

Ongoing surveys, such as DES, KiDS, HSC, and Extended Baryon Oscillation Spectroscopic Survey (eBOSS⁴), have played crucial roles in testing the Λ CDM model and constraining the cosmological parameters. In the next decade, upcoming galaxy surveys such as Vera C. Rubin Observatory (or LSST, Chisari et al. 2019; Ivezić et al. 2019), Nancy Grace Roman Space Telescope (RST) (or WFIRST, Akeson et al. 2019), Euclid (Laureijs et al. 2011; Amendola et al. 2013, 2018), and CSST (Zhan 2011, 2018, 2021; Gong et al. 2019), will explore an unprecedented large volume of the Universe, enabling us to test the cosmological model and probe the cosmological parameters with extraordinary precision.

The CSST is a 2 m space telescope, which will cover 17500 deg² survey area with multi-band photometric imaging and slitless grating spectroscopy. It can perform photometric and spectroscopic surveys simultaneously with high spatial and spectral resolutions. It has *NUV*, *u*, *g*, *r*, *i*, *z*, and *y* seven photometric imaging bands, which covers the wavelength range from 250 nm to 1000 nm. The 5σ point-source magnitude limits for the seven bands can achieve 25.4, 25.4, 26.3, 26.0, 25.9, 25.2, and 24.4 AB mag, respectively. The CSST spectroscopic observation is accomplished by slitless gratings, which contains *GU*, *GV*, and *GI* bands with the same wavelengths range and survey area as photometric observation. The corresponding magnitude limits are 23.2, 23.4, and 23.2, respectively. Since the CSST photometric and spectroscopic surveys will cover large and overlapping regions of the sky, they allow us to measure the growth and geometry of the Universe through a variety of cosmological probes, e.g. weak lensing (Troxel et al. 2018; Secco et al. 2022), photometric galaxy clustering (Elvin-Poole et al. 2018; Porredon et al. 2021), cluster number counts (Haiman et al. 2001; Lima & Hu 2005; Allen et al. 2011), Alcock-Paczynski (AP) effect (Alcock & Paczynski 1979; Li et al. 2014, 2019), redshift-space distortions (RSD, Gil-Marín et al. 2016a, 2017), BAO (Gil-Marín et al. 2016b; Beutler et al. 2017b; Rosell et al. 2022; Abbott et al. 2022b; Neveux et al. 2020; Gil-Marín et al. 2020), etc. The CSST will be a powerful survey instrument for probing expansion history and structure growth of the Universe. Especially, Combining various CSST cosmological probes will provide more robust and precise constraints on cosmological parameters.

In this paper we forecast the cosmological constraints from the CSST 3×2 pt, spectroscopic galaxy clustering, and cluster number counts surveys. The mock data are generated based on the CSST observational and instrumental designs, and related systematics are also considered. We use Fisher matrix to extract cosmological information and perform the prediction. The analysis of the CSST photometric 3×2 pt and spectroscopic galaxy clustering surveys are discussed in section 2 and 3, respectively. The number counts of galaxy clusters for the CSST is shown in section 4. The details of Fisher matrix analysis is given in section 5. We present our constraint results of cosmological and systematical parameters in section 6, and summarize the results in section 7.

2 3×2 PT ANALYSIS

The CSST is expected to obtain billions of high-resolution galaxy images, that enables us to study the weak gravitational lensing effect

¹ <http://www.astro-wisconsin.org/projects/KIDS/>

² www.darkenergysurvey.org/

³ <http://www.naoj.org/Projects/HSC/HSCProject.html>

⁴ <https://www.sdss.org/surveys/eboss>

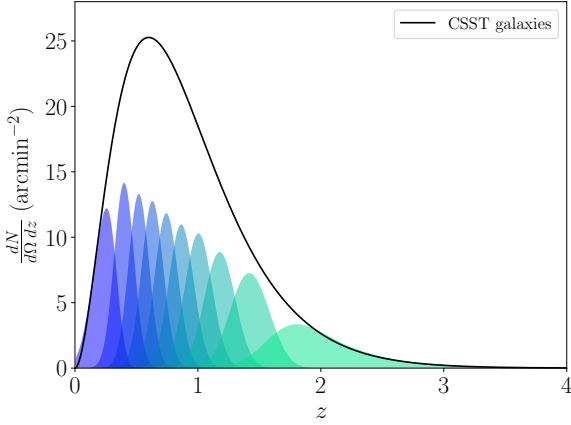


Figure 1. The galaxy redshift distribution of the CSST photometric survey. The total and 10 tomographic galaxy distributions are shown in black solid curve and filled regions, respectively.

and measure the evolution and formation of the LSS. Usually, the weak lensing effect is much smaller than the intrinsic irregularity of shapes and sizes of galaxies, and can not be detected in any single galaxy image. So we have to rely on statistical approaches to measure this signal (the so-called shear signal) from large galaxy samples, and extract the cosmological information encoded therein (Munshi et al. 2008; Hoekstra & Jain 2008; Kilbinger 2015; Mandelbaum 2018).

Besides the shape related information, the photometric observation also provides us with the spatial distribution information of galaxies (i.e. galaxy clustering). This enables us to perform the galaxy clustering analysis using the angular power spectra in tomographic photometric redshift bins (Weaverdyck & Huterer 2021; Rodríguez-Monroy et al. 2022). In case of the uncertainties of photo- z are well controlled, high precision cosmology results can be obtained (Tanoglidis et al. 2020; Hasan et al. 2022).

Furthermore, the cross-correlation between the lensing effect of sources and spatial distribution of lenses, known as the galaxy-galaxy lensing, (Baldauf et al. 2010; Heymans et al. 2013; Mandelbaum et al. 2013; Singh et al. 2017), serves as another complementary statistical method for the cosmological analysis. The cross-correlation approach has great advantages in mitigating critical sources of systematic errors, in particular the intrinsic alignment effects in the observed shear signal and galaxy bias (Mandelbaum et al. 2005; Clampitt et al. 2017; Giblin et al. 2021; Park et al. 2021b).

A combination of the above three methods leads to the so-called 3×2 pt method, which is widely applied in the analysis of ongoing observations (van Uitert et al. 2018; Heymans et al. 2021; Joachimi et al. 2021; Abbott et al. 2022a) and forecasts of near-future photometric surveys (Euclid Collaboration et al. 2020; Tutusaus et al. 2020; Zuntz et al. 2021). This combination approach is beneficial to breaking the degeneracy between cosmological parameters and galaxy bias, and also enables the self-calibration of the systematical and astrophysical parameters in a specific cosmological model. Therefore, in this work, we firstly study the application of the 3×2 pt method to the CSST photometric observation.

Following the CSST specifications given in Gong et al. (2019), we adopt the galaxy redshift distribution $n(z) \propto z^\alpha e^{-(z/z_0)^\beta}$, with $\alpha = 2$, $\beta = 1$, $z_0 = 0.3$, and choose a total number density $n = 28 \text{ arcmin}^{-2}$. We assume the same galaxy distribution for lenses and sources, since it can help to constrain the photo- z error (Schaan et al.

2020). To carry out a tomographic analysis, we divide the galaxy sample into 10 photo- z bins with identical galaxy number density per bin. The redshift distribution of the galaxies as well as our binning scheme is illustrated in Fig. 1⁵.

Photo- z uncertainty is one of the leading systematics in photometric observations (Hildebrandt et al. 2021; Stölzner et al. 2021; Rau et al. 2022). For modeling of the photo- z uncertainty, we assume that the true redshift distribution of a photometric tomographic bin is given by the conditional probability distribution $p(z_{\text{ph}}|z)$ at a given z (Ma et al. 2006), whose form in the i -th tomographic bin is described by

$$p^i(z_{\text{ph}}|z, x) = \frac{1}{\sqrt{2\pi}\sigma_z} \exp\left[-\frac{(z - z_{\text{ph}} - \delta_{z,x}^i)^2}{2\sigma_z^2}\right], \quad (1)$$

where $x \in \{g, \kappa\}$ (g and κ denote galaxy clustering and weak lensing surveys, respectively), $\delta_{z,x}^i$ is the photo- z bias, and the scatter parameter σ_z is characterized as

$$\sigma_z = \sigma_{z0}(1+z). \quad (2)$$

So the true redshift distribution of galaxies in a tomographic bin is given by

$$n_x^i(z) = \int_{z_{\text{min}}^i}^{z_{\text{max}}^i} dz_{\text{ph}} n_x(z) p^i(z_{\text{ph}}|z), \quad (3)$$

and the total surface number density of galaxies in a tomographic bin is

$$\bar{n}_x^i = \int dz n_x^i(z). \quad (4)$$

The angular power spectrum $C_{AB}^{ij}(\ell)$ is calculated under the flat sky assumption and Limber approximation (Kaiser & Squires 1993) between tomographic bin i of observable A and tomographic bin j of observable B, where A, B $\in \{g, \kappa\}$. It can be written as

$$C_{AB}^{ij}(\ell) = \int d\chi \frac{q_A^i(\chi) q_B^j(\chi)}{\chi^2} P_m\left(\frac{\ell + 1/2}{\chi}, z(\chi)\right), \quad (5)$$

where χ is the comoving radial distance, P_m is the non-linear matter power spectrum, and q_A^i are weight functions of the different observables. To constrain cosmological parameters with future high-precision data sets, the matter power spectrum must be modeled accurately. It has been found that the cosmic shear power spectrum is sensitive to a small scale until the wavenumber $k \simeq 7 \text{ h/Mpc}$ (Taylor et al. 2018). Our non-linear matter power spectrum P_m is calculated using the *halofit* code (Takahashi et al. 2012).⁶ For the galaxy clustering and galaxy-galaxy lensing angular power spectrum,

⁵ Here we stress that the cosmological results are dependent on the bin width (Hu 1999; Zhan 2006; Asorey et al. 2012; Tanoglidis et al. 2020; Hasan et al. 2022), and increasing the number of bins is always beneficial unless the bin widths are smaller than the individual photo- z scatter. In addition, the scheme of an equal number of galaxies per bin can capture more information than equally spaced bins in redshift (see e.g. Taylor et al. 2018). We will discuss this complicated issue in future works.

⁶ Here we do not consider the baryonic effects on the non-linear power spectrum, which are important and have been studied extensively (Mead et al. 2015, 2016, 2021; Copeland et al. 2018; Schneider et al. 2019; Huang et al. 2019; Martinelli et al. 2021). We should note that if baryonic effects are considered, the results of weak lensing constraint on cosmological parameters may be degraded based on Fisher analysis (see e.g. Copeland et al. 2018). We will study the baryonic effects particularly in our future work.

we only consider the multipoles that satisfy $\ell \leq k_{\max} \chi(z_i) - 1/2$, where z_i represents the mean value of redshift bin i . We have set $k_{\max} = 0.3 h/\text{Mpc}$ in the CSST photometric galaxy clustering and galaxy-galaxy lensing surveys to avoid the non-linear effects (Schaan et al. 2020).

The weight function of the galaxy clustering and weak lensing are given by

$$q_g^i(k, \chi) = b^i(k, z(\chi)) \frac{n_g^i(z(\chi))}{\bar{n}_g^i} \frac{dz}{d\chi}, \quad (6)$$

$$q_k^i(\chi) = \frac{3H_0^2 \Omega_m}{2c^2} \frac{\chi}{a(\chi)} \int_{\chi}^{\chi_h} d\chi' \frac{n_k^i(z(\chi'))}{\bar{n}_k^i} \frac{dz/d\chi'}{\chi' - \chi}, \quad (7)$$

where b_i is the linear galaxy bias in the i th bin, c is the speed of light, a is the scale factor, H_0 is the Hubble constant, and χ_h is the line-of-sight comoving horizon distance.

The shear signal is coherent with intrinsic alignment (IA) effect. If galaxy shapes are randomly oriented, IA will not affect the results of shear analysis. However, because of the local tidal fields and gravitational interactions between galaxies, IA leads to an additional term for the shear signal. Therefore the IA must be modeled in our observed shear signal. The exact form of IA is related to galaxy formation and evolution, and also halo models (Joachimi et al. 2015; Kiessling et al. 2015; Kirk et al. 2015; Troxel & Ishak 2015). Due to the uncertainty of those processes, IA is typically predicted by linking observed galaxy shapes to the gravitational tidal field in the LSS based on tidal alignment or tidal torquing models (Hirata & Seljak 2004; Bridle & King 2007; Blazek et al. 2011). We assume the tidal alignment model in our analysis, which describes the shape alignments of red elliptical galaxies in the tidal field. It captures the primary IA effect, and ignores the tidal torquing mechanism and secondary alignment of blue spiral galaxies (Blazek et al. 2019; Samuroff et al. 2019). When IA is considered, the galaxy lensing weight function can be modeled as (Kirk et al. 2012; Krause et al. 2016)

$$q_k^i(\chi) \longrightarrow q_k^i(\chi) - A(z(\chi)) \frac{n_k^i(z(\chi))}{\bar{n}_k^i} \frac{dz}{d\chi}. \quad (8)$$

Then the final shear power spectrum will contain the auto-correlation of IA between neighboring galaxies, and the cross-correlation between the IA of foreground lens and shear signals of background sources. The function $A(z(\chi))$ can be expressed as

$$A(z) = A_{\text{IA}} C_1 \rho_{\text{cr}} \frac{\Omega_m}{D(z)} \left(\frac{1+z}{1+z_0} \right)^{\alpha_{\text{IA}}} \left(\frac{L}{L_0} \right)^{\beta_{\text{IA}}}, \quad (9)$$

where A_{IA} is intrinsic alignments amplitude, ρ_{cr} is the present critical density and we have $C_1 \rho_{\text{cr}} = 0.0134$, $z_0 = 0.62$ is the pivot redshift, $D(z)$ is the growth factor, α_{IA} and β_{IA} represent the relations of redshift and luminosity, respectively. For simplicity, we fix $\beta_{\text{IA}} = 0$ for ignoring the dependence of luminosity.

In addition to IA, the process of estimating shear signals from galaxy shapes also leads to additional biases, which are commonly described as the additive and multiplicative errors (Huterer et al. 2006; Heymans et al. 2006; Massey et al. 2013). To satisfy the requirements of future weak lensing surveys, the additive and multiplicative errors need to be smaller than 10^{-3} and 0.03 at least, respectively. In particular, the multiplicative bias degenerates with the shear amplitude, and can significantly affect the accuracy of shear measurements. Many uncertainties can result in multiplicative bias (Jarvis et al. 2016; Fenech Conti et al. 2017), such as errors from point spread function (PSF) modeling size, select bias, galaxy shape

measurement, or detector systematics (Paulin-Henriksson et al. 2008; Mandelbaum 2018; Pujol et al. 2020a). Since the upcoming Stage IV weak lensing survey will measure the shear signal with an unprecedented level of accuracy, shear biases must be calibrated precisely (Taylor & Kitching 2018; Gillis & Taylor 2019). For example, the multiplicative bias can be self-calibrated by cross-correlation with CMB lensing (Vallinotto 2012; Das et al. 2013; Schaan et al. 2017), and machine learning method also can be used in the calibration (Pujol et al. 2020b). We consider the multiplicative shear calibration in our analysis and describe it as one parameter m^i in tomographic redshift bin i . For the weak lensing survey and galaxy-galaxy lensing survey, we have

$$C_{\kappa\kappa}^{ij}(\ell) \longrightarrow (1+m^i)(1+m^j) C_{\kappa\kappa}^{ij}(\ell),$$

$$C_{g\kappa}^{ij}(\ell) \longrightarrow (1+m^j) C_{g\kappa}^{ij}(\ell). \quad (10)$$

For galaxy clustering survey, the linear galaxy bias is modeled using one nuisance parameter in a tomographic redshift bin. The fiducial values of galaxy bias is given by $b(z) = 1 + 0.84z$ (Zhan 2006). Besides, since the measured power spectra also subject to galaxy shot noise and other systematic noises, and then we have

$$\tilde{C}_{\kappa\kappa}^{ij}(\ell) = C_{\kappa\kappa}^{ij}(\ell) + \delta_{ij}^K \frac{\sigma_\epsilon^2}{\bar{n}_k^i} + N_{\kappa\kappa}, \quad (11)$$

$$\tilde{C}_{gg}^{ij}(\ell) = C_{gg}^{ij}(\ell) + \delta_{ij}^K \frac{1}{\bar{n}_g^i} + N_{gg}, \quad (12)$$

where δ_{ij}^K is Kronecker delta function, σ_ϵ^2 is the variance of the observed ellipticities, $N_{\kappa\kappa}$ and N_{gg} are systematic noises that may be generated from the PSF, photometry offsets, instrumentation effects, dust extinction, and so on (Tegmark et al. 2002; Jain et al. 2006). Here, we just simply assume $N_{\kappa\kappa} = 10^{-9}$ and $N_{gg} = 10^{-8}$ (Zhan 2006; Huterer et al. 2006; Gong et al. 2019), and $\sigma_\epsilon = 0.3$ in our analysis.

3 SPECTROSCOPIC GALAXY CLUSTERING

Besides photometric imaging survey, the CSST can also perform slit-less spectroscopic galaxy survey simultaneously, and more than one hundred million galaxy spectra (mainly from emission line galaxies) can be obtained (Gong et al. 2019). Based on the zCOSMOS catalog (Lilly et al. 2009), we simulate the mock catalog of CSST spectroscopic galaxy survey, and divide the redshift range from $z = 0$ to 1.5 into five bins for studying evolution of important cosmological parameters, such as the equation of state of dark energy. The details can be found in Gong et al. (2019). The expected galaxy number density distribution of the CSST spectroscopic survey has been shown in Fig. 2, and the details of surface and volume number densities and galaxy bias in each spec- z bins are given in Table 1.

From the current spectroscopic galaxy surveys, such as the 2-degree Field Galaxy Redshift Survey (2dFGRS, Cole et al. 2005) to 6-degree Field Galaxy Survey (6dFGS, Jones et al. 2009), WiggleZ Dark Energy Survey (WiggleZ, Parkinson et al. 2012) then to SDSS-III Brayon Oscillation Spectroscopic Survey (BOSS, Dawson et al. 2013) and SDSS-IV extended BOSS (eBOSS, Dawson et al. 2016), we can acquire a wealth of information to understand our Universe. The BAO and RSD signals from these surveys have been analyzed particularly by using different methods (Beutler et al. 2017b,a; Gil-Marín et al. 2020; Foroozan et al. 2021). One can obtain important

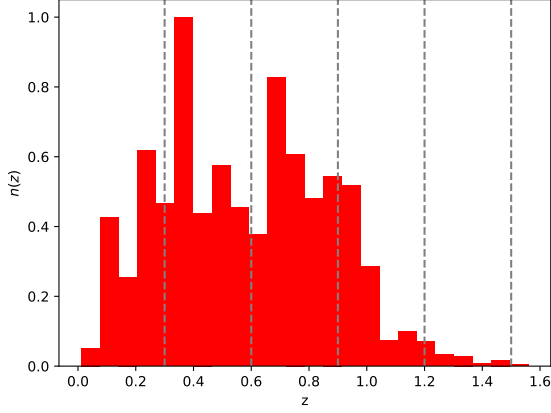


Figure 2. Galaxy number density distribution of the CSST slitless spectroscopic survey. The vertical grey dashed lines denote the five spec- z bins we divide for cosmic evolution study.

Table 1. Galaxy surface and volume number densities, and galaxy biases for the five spec- z bins in the CSST spectroscopic survey.

z_{\min}	z_{\max}	z_{mean}	$dN(z)/d\Omega dz [\text{arcmin}^{-2}]$	$\bar{n}(z) [h^3 \text{Mpc}^{-3}]$	$b(z)$
0	0.3	0.15	1.54	2.81×10^{-2}	1.126
0.3	0.6	0.45	3.35	1.16×10^{-2}	1.378
0.6	0.9	0.75	3.16	5.63×10^{-3}	1.63
0.9	1.2	1.05	0.9	1.15×10^{-3}	1.882
1.2	1.5	1.35	0.09	9.65×10^{-5}	2.134

information of the LSS and dark energy from the BAO wiggles of the galaxy power spectrum (Seo & Eisenstein 2007; Font-Ribera et al. 2014), or the full shape of the power spectrum which contains more information.

In a real spectroscopic survey, we are actually observing the distribution of galaxies in redshift space. The observed galaxy redshift always contains an additional contribution by the peculiar velocity of the galaxy, which can be expressed by

$$1 + z_{\text{obs}} = (1 + z)(1 + v_{\parallel}/c), \quad (13)$$

where v_{\parallel} denotes the peculiar velocity of a galaxy along the light of sight. This term will lead to the redshift-space clustering anisotropic of galaxy distribution, or so-called RSD (Hamilton 1998). The relation between real and redshift space galaxy power spectrum has been given in linear regime (Kaiser 1987). When analyzing galaxy distribution from galaxy surveys, we must assume a fiducial cosmological model to transform observed angular positions and redshift into physical coordinates. If we adopt a wrong fiducial cosmology, an extra anisotropic clustering signal will be introduced. This distortion, which is called AP effect, is different from RSD and also can be used to constrain cosmological parameters (Marinoni & Buzzi 2010; López-Corredoira 2014; Li et al. 2018, 2019). Here the linear galaxy bias $b(z)$, RSD, and AP effect are considered, and the galaxy power spectrum can be written as

$$P_{\text{obs}}(k_{\text{ref}}, \mu_{\text{ref}}; z) = \frac{1}{q_{\perp}^2 q_{\parallel}} \left(b(z) \sigma_8(z) + f \sigma_8(z) \mu^2 \right)^2 \frac{P_{\text{m}}(k; z)}{\sigma_8^2(z)} \times e^{-k^2 \mu^2 \sigma_r^2(z) + P_s(z)}, \quad (14)$$

where $f = d \ln D(a) / d \ln a$ is the growth rate, $P_s(z)$ is the shot noise term, and $P_{\text{m}}(k; z)$ is the matter power spectrum. Here only the linear matter power spectrum is considered, which can be obtained by CAMB (Lewis et al. 2000). The radial smearing factor $\sigma_r(z)$ is induced by spec- z error and can be estimated as

$$\sigma_r(z) = \frac{\partial r}{\partial z} \sigma_z(z) = \frac{c}{H(z)} (1 + z) \sigma_{0,z}, \quad (15)$$

where $\sigma_z(z) = \sigma_{0,z}(1 + z)$, and $\sigma_{0,z}$ is the error of redshift measurement. The k and μ of eq. (14) are given by

$$k(k_{\text{ref}}, \mu_{\text{ref}}) = \frac{k_{\text{ref}}}{q_{\perp}} \left[1 + \mu_{\text{ref}}^2 \left(\frac{q_{\perp}^2}{q_{\parallel}^2} - 1 \right) \right]^{1/2},$$

$$\mu(\mu_{\text{ref}}) = \mu_{\text{ref}} \frac{q_{\perp}}{q_{\parallel}} \left[1 + \mu_{\text{ref}}^2 \left(\frac{q_{\perp}^2}{q_{\parallel}^2} - 1 \right) \right]^{-1/2}. \quad (16)$$

where

$$q_{\perp}(z) = \frac{D_A(z)}{D_{A,\text{ref}}(z)}, \quad q_{\parallel}(z) = \frac{H_{\text{ref}}(z)}{H(z)},$$

$$k_{\perp} = \frac{k_{\perp,\text{ref}}}{q_{\perp}} \quad \text{and} \quad k_{\parallel} = \frac{k_{\parallel,\text{ref}}}{q_{\parallel}}. \quad (17)$$

The indicator ‘ref’ denotes the referenced cosmology, and $D_A(z)$ and $H(z)$ represent the angular diameter distance and Hubble parameter, respectively. For the galaxy power spectrum, we do not consider non-linear effects, since we are focusing on linear scales here. Galaxy bias is modeled as $b(z) = 1 + 0.84z$, the redshift uncertainty is assumed to be $\sigma_{0,z} = 0.002$ for the CSST, and shot noise $P_s(z) = 1/\bar{n}$. Besides, we also add a constant systematics term, $N_{\text{sys}} = 5 \times 10^4 (\text{Mpc}/h)^3$, in galaxy power spectrum to consider instrumentation effects (Gong et al. 2019).

4 CLUSTER NUMBER COUNTS

Galaxy cluster abundance or number counts is another important probe in the CSST survey. Clusters can be detected at different bands with various methods, including X-ray, optical, and sub-mm bands (Koester et al. 2007; Rozo et al. 2015; Sunyaev & Zeldovich 1972), and cluster abundance is a powerful tool in cosmological studies. However, accurately identifying cluster members and determining cluster mass are still challenging in current galaxy surveys, which are crucial in the studies of number counts of galaxy clusters. A class of methods for finding galaxy clusters and estimating their mass in optical surveys is based on the presence of a red sequence of galaxies, such as maxBCG (Koester et al. 2007), redMaPPer (Rykoff et al. 2014) used in DES (Rykoff et al. 2016), and CAMIRA (Oguri 2014) applied in HSC (Oguri et al. 2018). Besides, a different approach, e.g. AMICO (Bellagamba et al. 2018), which is based on the optimal filtering technique, has been used in KiDS (Bellagamba et al. 2019; Lesci et al. 2022b). Usually, the cluster mass can be measured using observational proxies that can be related to mass. In optical surveys, cluster richness and gravitational lensing effect often serve as mass tracers (Roza et al. 2009; Rykoff et al. 2012). Based on the mass-observable relations or so-called scaling relations, one can estimate the cluster mass in an individual or statistical way (Roza et al. 2010; Abdullah et al. 2020; Costanzi et al. 2021; Lesci et al. 2022a).

The CSST can perform photometric and spectroscopic surveys simultaneously, which is powerful to identify galaxy clusters and their members, and measure their redshifts and masses. Here we derive the CSST number counts of galaxy clusters from the halo mass function, which is given by (Press & Schechter 1974; Sheth &

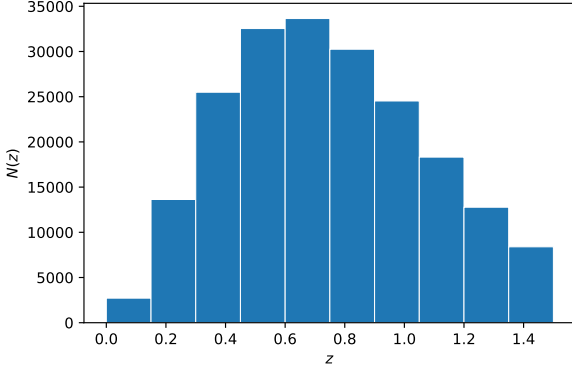


Figure 3. The expected redshift distribution of number counts of galaxy clusters in the CSST survey. The redshift range we consider from $z = 0$ to 1.5 has been divided into 10 bins.

(Tormen 1999; Tinker et al. 2008)

$$\frac{dn(M, z)}{d \ln M} = \frac{\bar{\rho}_m}{M} f(\sigma) \frac{d \ln \sigma^{-1}}{d \ln M}, \quad (18)$$

where $\bar{\rho}_m$ is the mean matter density, and

$$\sigma^2(R) = \frac{1}{2\pi^2} \int dk k^2 P(k) W_R^2(k). \quad (19)$$

Here $R = (3M/4\pi\bar{\rho}_m)^{1/3}$ is the smoothing scale, $W(k, R) = \frac{3}{(kR)^3} (\sin kR - (kR) \cos kR)$ is the window function. The multiplicity function is given by (Tinker et al. 2008)

$$f(\sigma) = A \left[\left(\frac{\sigma}{b} \right)^{-a} + 1 \right] e^{-c/\sigma^2}, \quad (20)$$

where the parameters A , a , b , and c depend on the redshift and halo mass definition and can be determined by simulations.

The expected values of cluster number counts in the i -th mass bin and α -th redshift bin is then given by

$$N_{\alpha i} = \int_{\Delta z_\alpha} dz \frac{dV}{dz} \int_{\Delta M_i} dM \frac{dn}{dM}(M, z). \quad (21)$$

Here,

$$\frac{dV}{dz} = \Delta\Omega \left(\frac{\pi}{180} \right)^2 \frac{c}{H(z)} \left(\int_0^z dz' \frac{c}{H(z')} \right)^2, \quad (22)$$

where $\Delta\Omega$ is the survey area in square degrees. We use the public CCL code (Chisari et al. 2019) to calculate the cluster abundance. For the CSST, to accurately measure the redshifts and masses of galaxy clusters, we only consider the redshift range from $z = 0$ to 1.5 , which can be covered by both of CSST photometric and spectroscopic surveys. This redshift range is equally divided by 10 bins to study the evolution of the Universe. We consider the cluster halo mass range from $10^{14} h^{-1} M_\odot$ to $10^{16} h^{-1} M_\odot$ in the estimation. We find that the CSST could detect about 170,000 clusters in 17500 deg^2 survey area. The redshift distribution of the number counts of CSST galaxy clusters has been shown in Fig. 3. We find that the CSST cluster redshift distribution has a peak around $z = 0.6$, and can extend to $z \sim 2$.

Besides the statistical uncertainties including shot noise and sample variance, the uncertainties of cluster number counts mainly come from observational uncertainties related to mass measurements, such as photometric/spectroscopic noise, background subtraction, and projection/percolation effects (see e.g. Costanzi et al. 2019). We will discuss these uncertainties in details in the next section.

5 FISHER MATRIX FORECAST

We adopt Fisher matrix to predict the constraint results from the cosmological multi-probes in the CSST photometric and spectroscopic surveys. We assume the Likelihood function to be Gaussian and is given by

$$\ln L(\vec{D}|\vec{\theta}) = -\frac{1}{2} (\vec{D} - \vec{M}(\vec{\theta}))^T \Sigma^{-1} (\vec{D} - \vec{M}(\vec{\theta})), \quad (23)$$

where \vec{D} is the data vector, $\vec{M}(\vec{\theta})$ is the corresponding predicted vector from theoretical model given the parameter vector $\vec{\theta}$, and Σ is the covariance matrix. Then the Fisher matrix is defined as (Tegmark et al. 1997)

$$F_{\theta_\alpha \theta_\beta} = \left\langle - \frac{\partial^2 \ln L}{\partial \theta_\alpha \partial \theta_\beta} \right\rangle_{\theta_0}, \quad (24)$$

where the derivatives are calculated in the point θ_0 of the parameter space. If assuming the covariance matrix is independent of the parameters, which should be available for most cases (Carron 2013), it can be rewritten as

$$F_{\theta_\alpha \theta_\beta} = \frac{\partial M^T}{\partial \theta_\alpha} \Sigma^{-1} \frac{\partial M}{\partial \theta_\beta}. \quad (25)$$

Besides, we can easily get a new Fisher matrix for a set of new parameters $\vec{p}(\vec{\theta})$ by performing Jacobian transform

$$S_{p_i p_j} = \sum_{\alpha\beta} \frac{\partial \theta_\alpha}{\partial p_i} F_{\theta_\alpha \theta_\beta} \frac{\partial \theta_\beta}{\partial p_j}. \quad (26)$$

In our forecast, the final adopted cosmological parameters for the three CSST cosmological probes are

$$\vec{\theta} = \{\Omega_m, \Omega_b, w_0, w_a, h, n_s, \sigma_8\}, \quad (27)$$

and the fiducial values of those cosmological parameters are assumed to be $(0.314, 0.0494, -1, 0, 0.6732, 0.966, 0.82)$.

5.1 Forecast for photometric 3×2 pt surveys

In the case of 3×2 pt analysis, the covariance matrix can be expressed as a four point function, and it can be estimated as

$$\begin{aligned} \text{Cov}_{AB A' B'}^{(ijkl)}(\ell) &\equiv \text{Cov} \left[\tilde{C}_{AB}^{ij}(\ell), \tilde{C}_{A' B'}^{kl}(\ell') \right] \\ &= \frac{\tilde{C}_{AA'}^{ik}(\ell) \tilde{C}_{BB'}^{jl}(\ell') + \tilde{C}_{AB'}^{il}(\ell) \tilde{C}_{BA'}^{jk}(\ell')}{(2\ell + 1) f_{\text{sky}} \Delta\ell} \delta_{\ell\ell'}^K. \end{aligned} \quad (28)$$

Here f_{sky} is the sky survey fraction, which is about 42% for the CSST survey. The data vector of the observed weak lensing, galaxy-galaxy lensing, and angular galaxy power spectra D^T is given by

$$\begin{aligned} D^T &= \left\{ \tilde{C}_{\kappa\kappa}^{(11)}(\ell), \dots, \tilde{C}_{\kappa\kappa}^{(N_{\text{zbin}} N_{\text{zbin}})}(\ell), \tilde{C}_{g\kappa}^{(11)}(\ell), \tilde{C}_{g\kappa}^{(N_{\text{zbin}} N_{\text{zbin}})}(\ell), \right. \\ &\quad \left. \tilde{C}_{gg}^{(11)}(\ell), \dots, \tilde{C}_{gg}^{(N_{\text{zbin}} N_{\text{zbin}})}(\ell) \right\}, \end{aligned} \quad (29)$$

and the corresponding covariance is written as

$$\text{Cov}(\ell) = \begin{pmatrix} \text{Cov}_{\kappa\kappa\kappa\kappa}^{(ijkl)}(\ell) & \text{Cov}_{\kappa\kappa g\kappa}^{(ijkl)}(\ell) & \text{Cov}_{\kappa\kappa gg}^{(ijkl)}(\ell) \\ \text{Cov}_{g\kappa\kappa\kappa}^{(ijkl)}(\ell) & \text{Cov}_{g\kappa g\kappa}^{(ijkl)}(\ell) & \text{Cov}_{g\kappa gg}^{(ijkl)}(\ell) \\ \text{Cov}_{gg\kappa\kappa}^{(ijkl)}(\ell) & \text{Cov}_{gg g\kappa}^{(ijkl)}(\ell) & \text{Cov}_{gg gg}^{(ijkl)}(\ell) \end{pmatrix}. \quad (30)$$

Table 2. The ℓ -cut in galaxy clustering angular power spectrum.

z_{bin}	z_{mean}	ℓ_{max}	N_{ℓ}^{max}
1	0.165	211	21
2	0.395	476	30
3	0.515	601	33
4	0.625	707	34
5	0.74	811	36
6	0.865	916	37
7	1.0	1025	38
8	1.18	1149	40
9	1.44	1312	41
10	2.8	1894	45

Then the final Fisher matrix is

$$F_{\theta_{\alpha}\theta_{\beta}} = \sum_{m,n}^{N_D} \sum_{\ell}^{N_{\ell}^{\text{max}}(m,n)} \frac{\partial D_n^T(\ell)}{\partial \theta_{\alpha}} \text{Cov}_{mn}^{-1}(\ell) \frac{\partial D_n(\ell)}{\partial \theta_{\beta}}, \quad (31)$$

where N_D is the dimension of data vector, N_{ℓ}^{max} is the available multipole mode bins.

The Fisher matrix analysis of the 3×2pt is completed by using COSMOSIS (Zuntz et al. 2015). To compute the Fisher matrix, we use $N_{\ell} = 50$ logarithm-spaced multipole bins between $\ell = 30$ and $\ell = 3000$. To avoid non-linear effect, we also remove the data at wavenumber $k_{\text{max}} = 0.3 \text{ h/Mpc}$ in the photometric galaxy clustering and galaxy-galaxy lensing surveys. The corresponding ℓ_{max} and N_{ℓ}^{max} of the 10 redshift tomographic bins are listed in Table 2. Besides the cosmological parameters, we also consider the systematic parameters in the 3×2pt analysis, including the photo- z bias, photo- z scatter, intrinsic alignment, galaxy bias, and shear calibration errors. Their fiducial values are given by $\Delta_z^i = 0$, $\sigma_{z_0} \sim N(\text{mean} = 0.05, \sigma = 0.003)$ (Normal distribution) (Ma et al. 2006; Schaun et al. 2020), $A_{\text{IA}} = 1$, $\alpha_{\text{IA}} = 0$, $b_i = 1 + 0.84z_i$, and $m_i = 0$, respectively.

5.2 Forecast for spectroscopic galaxy clustering survey

As listed in Table 1, in the analysis of the CSST spectroscopic galaxy clustering survey, we divide the redshift range from $z = 0$ to 1.5 into 5 tomographic redshift bins. In order to calculate Fisher matrix, we take the following cosmological parameters, i.e. shape parameters related to the shape of matter power spectrum $\{\Omega_b, \Omega_m, h, n_s\}$, and redshift-dependent parameters $\{\ln D_A(z_i), \ln H(z_i), \ln[f\sigma_8(z_i)], \ln[b\sigma_8(z_i)], P_s(z_i)\}$ (Wang et al. 2013; Euclid Collaboration et al. 2020). Note that the constraints on the other parameters, e.g. equation of state of dark energy w_0 and w_a , can be derived from the shape and redshift-dependent parameters by transferring the Fisher matrix into new ones using Eq.(26).

The Fisher matrix for spectroscopic galaxy surveys in a redshift bin is given by Tegmark (1997)

$$F_{\theta_{\alpha}\theta_{\beta}}^{\text{bin}}(z_i) = \frac{1}{8\pi^2} \int_{-1}^1 d\mu \int_{k_{\text{min}}}^{k_{\text{max}}} dk k^2 V_{\text{eff}}(z_i; k, \mu) \left[\frac{\partial \ln P_{\text{obs}}(k, \mu; z_i)}{\partial \theta_{\alpha}} \frac{\partial \ln P_{\text{obs}}(k, \mu; z_i)}{\partial \theta_{\beta}} \right], \quad (32)$$

where the effective survey volume is given by

$$V_{\text{eff}}(k, \mu; z) = V_s(z) \left[\frac{n(z)P_{\text{obs}}(k, \mu; z)}{n(z)P_{\text{obs}}(k, \mu; z) + 1} \right]^2. \quad (33)$$

The total Fisher matrix of all redshift bins then can be estimated by

$$F_{\theta_{\alpha}\theta_{\beta}} = \sum_{i=1}^{N_{z_{\text{bin}}}} F_{\theta_{\alpha}\theta_{\beta}}^{\text{bin}}(z_i). \quad (34)$$

Here the scale range is taken from $k = 0.001 \text{ h/Mpc}$ to 0.2 h/Mpc to avoid the non-linear effect (Huang et al. 2012).

5.3 Forecast for cluster number counts

The uncertainties of cluster number counts are mainly from the statistical uncertainties of shot noise and sample variance, and the systematical uncertainties in the measurements related to cluster mass determination. For simplicity, we only consider the shot noise term and a constant systematical error that includes all systematics that affect the mass measurement. In order to calculate Fisher matrix of cluster numbers, we assume the covariance matrix is given by

$$\text{Cov} = C_{\alpha\beta ij}^{\text{SN}} + C_{\text{sys}}, \quad (35)$$

where

$$C_{\alpha\beta ij}^{\text{SN}} = N_{\alpha i} \delta_{\alpha\beta} \delta_{ij}, \quad (36)$$

and C_{sys} is assumed to be 30% of $C_{\alpha\beta ij}^{\text{SN}}$ or the number of galaxy clusters in a redshift bin α and mass bin i . This constant systematics are estimated by the current photometric surveys (see e.g. Costanzi et al. 2019), which should be conservative for the CSST photometric and spectroscopic galaxy cluster surveys. The Fisher matrix then is written as

$$F_{\theta_m\theta_n} = \sum_{ai} \frac{\partial N_{ai}}{\partial \theta_m} \text{Cov}^{-1} \frac{\partial N_{ai}}{\partial \theta_n}. \quad (37)$$

6 RESULTS AND DISCUSSION

We present the marginalized 1σ and 2σ (i.e. 68.3% and 95.4% confidence levels, respectively) contour maps and probability distribution functions (PDFs) of the seven cosmological parameters in Fig. 4 and 5. Fig. 4 shows the results from CSST 3×2pt, spectroscopic galaxy clustering and cluster number counts surveys, respectively, and Fig. 5 shows the joint fitting results with all of these three probes. The joint fitting results are calculated by using the total Fisher matrix, which is given by $F_{\text{tot}} = F_{3\times 2\text{pt}} + F_{\text{spec-}z} + F_{\text{cluster}}$. We have marginalized all the systematical parameters to obtain these contour maps. The details of the forecast results of 1σ error and relative accuracy (the ratio of 1σ error to the fiducial value) for the seven cosmological parameters with different data sets are listed in Table 3. The ratios of 1σ errors to the fiducial values of the seven cosmological parameters for the CSST 3×2pt, spectroscopic galaxy clustering, and cluster number counts surveys are shown in Fig. 6 for comparison.

In the 3×2pt analysis, we find that the 1σ errors (and relative accuracies) of the constraint results on w_0 , w_a , Ω_m and σ_8 are given by $\sigma_{w_0} = 0.08$ (8%), $\sigma_{w_a} = 0.27$ (27%), $\sigma_{\Omega_m} = 0.01$ (3%) and $\sigma_{\sigma_8} = 0.009$ (1%), respectively. Comparing to the present photometric surveys, e.g. DES (Abbott et al. 2022a), our constraints on the dark matter related parameters Ω_m and σ_8 are improved by a factor of 3-5, and a factor of ~ 4 better for the equation of state of dark energy. This is due to that the CSST photometric surveys have larger survey area, deeper magnitude limit, and wider wavelength coverage with seven bands, which could significantly reduce the uncertainties from cosmic variance, Poisson noise, and photo- z calibration. Besides, CSST has higher imaging quality with a high spatial resolution $\sim 0.15''$

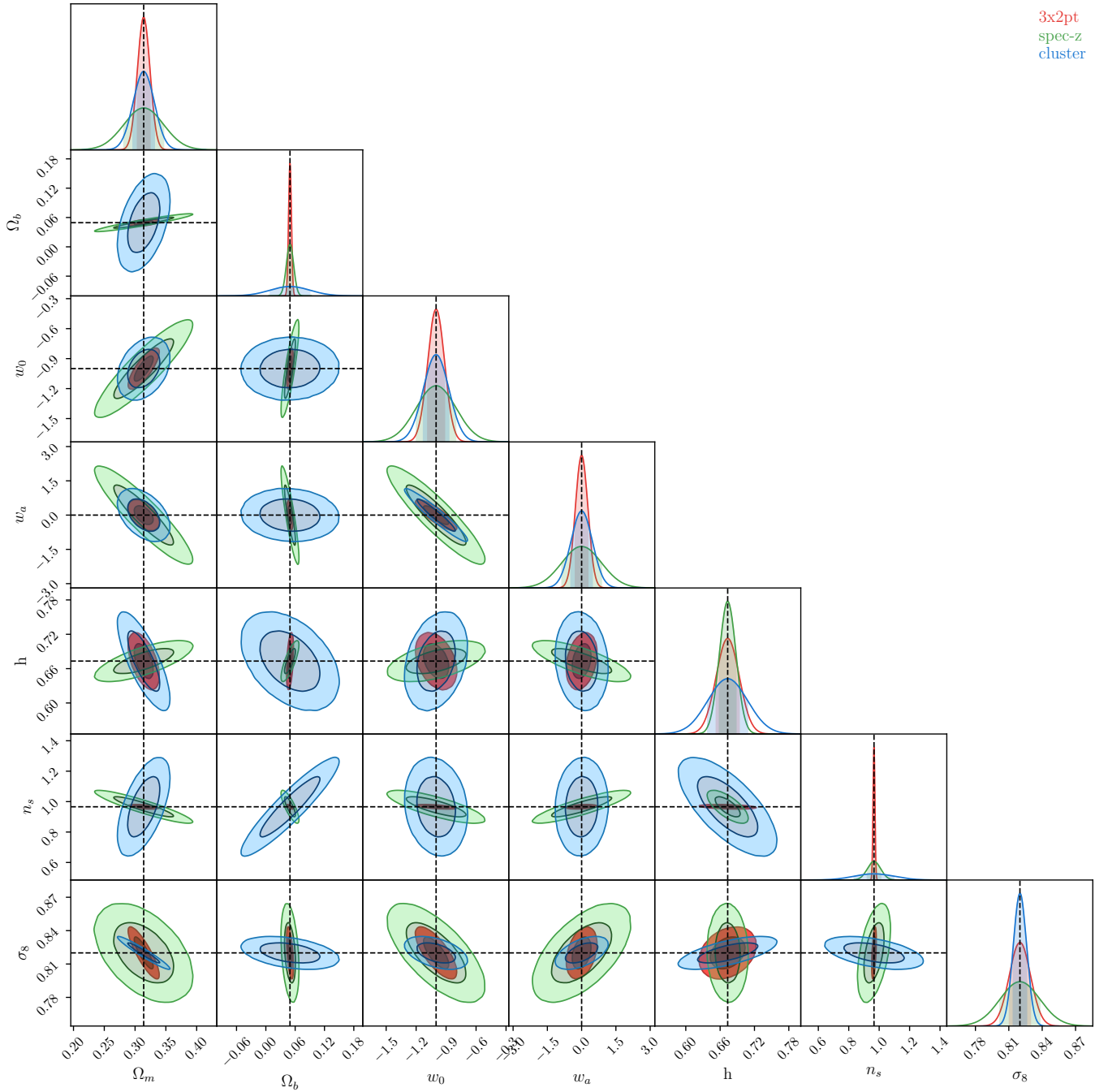


Figure 4. Marginalized posterior contour maps (1σ and 2σ) and 1D PDFs of the seven cosmological parameters for the CSST 3×2pt, spectroscopic galaxy clustering, and cluster number counts surveys, respectively.

(80% energy concentration region) and a Gaussian-like PSF (Gong et al. 2019; Zhan 2021). All of these advantages can be helpful to significantly improve the constraints on the cosmological parameters. Note that we do not consider the magnification effects here, which may lead to large biases but negligible errors for the constraint results (Unruh et al. 2020; Thiele et al. 2020; Duncan et al. 2022; Euclid Collaboration et al. 2022; Mahony et al. 2022).

For the CSST spectroscopic galaxy clustering survey, we get $\sigma_{w_0} = 0.2$ (20%), $\sigma_{w_a} = 0.86$ (86%), $\sigma_{\Omega_m} = 0.032$ (10%) and $\sigma_{\sigma_8} = 0.0177$ (2%). Compared to the current spectroscopic sur-

veys, e.g. BOSS (Alam et al. 2021), our constraint results of these cosmological parameters are improved by factors of ~ 2 -5 at least. This is mainly because of larger survey area and deeper magnitude limit in the CSST spectroscopic surveys, that much larger effective survey volume can be obtained to effectively reduce the statistical uncertainties. Although the spectral resolution in the CSST slitless spectroscopic survey is relatively low ($R \approx 200$), which may lead to a low spec- z accuracy, it would not significantly affect the 3D galaxy clustering measurements in the linear regime, given that the spec- z

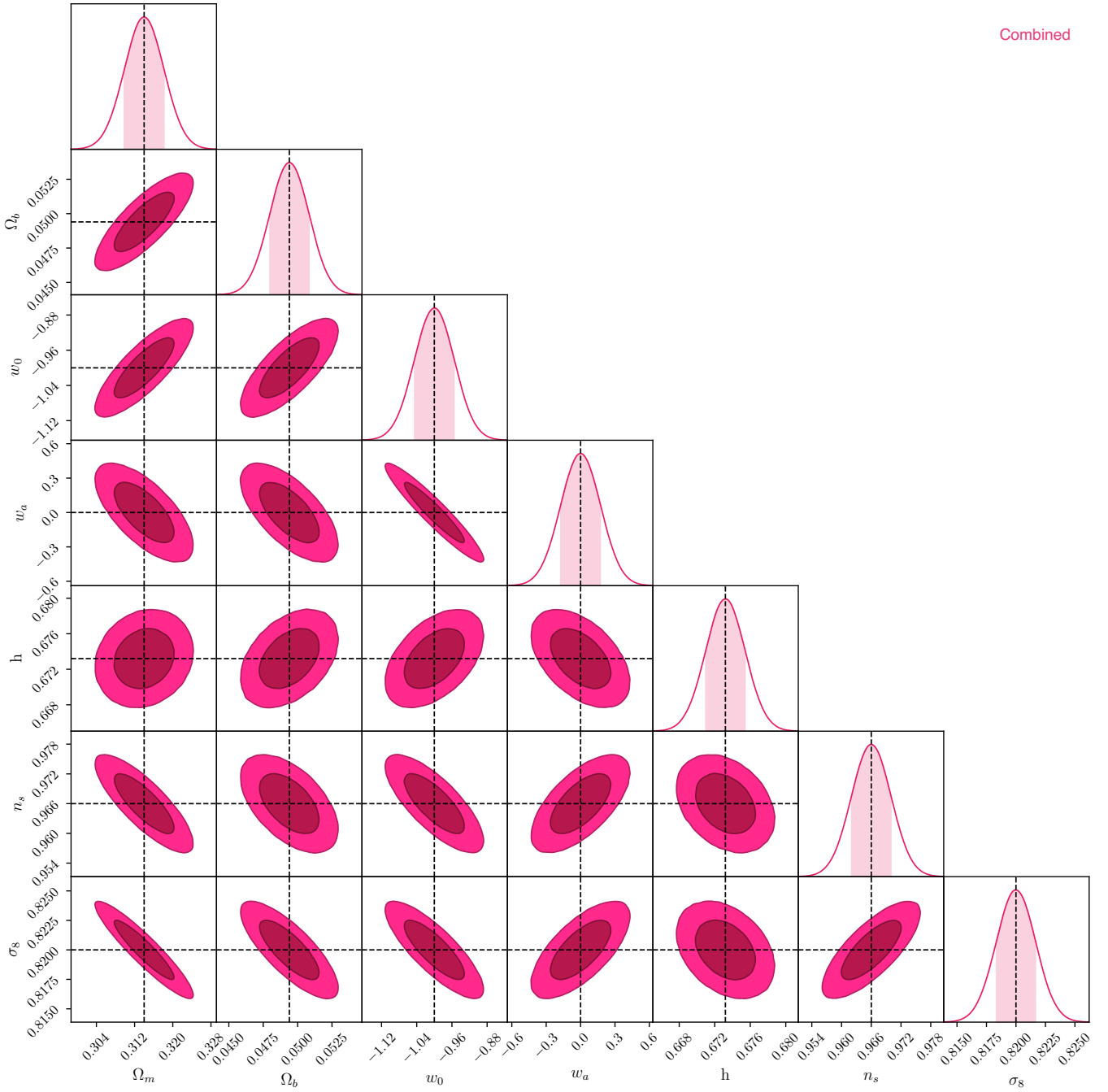


Figure 5. Marginalized posterior contour maps (1σ and 2σ) and 1D PDFs of the seven cosmological parameters for the joint constraints of all three probes.

accuracy is expected to be able to achieve 0.002-0.003 using the joint analysis with the CSST photometric data.

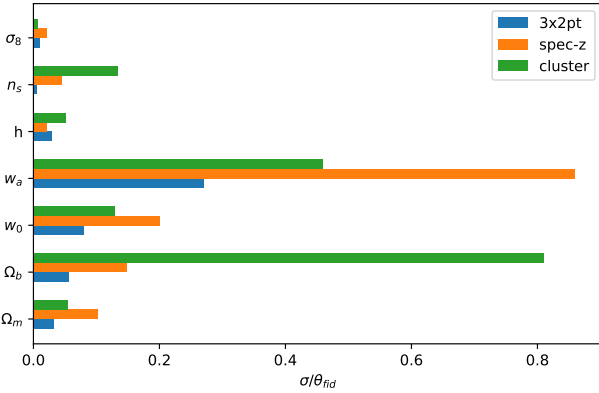
In the CSST cluster number counts survey, we obtain $\sigma_{w_0} = 0.13$ (13%), $\sigma_{w_a} = 0.46$ (46%), $\sigma_{\Omega_m} = 0.017$ (5%) and $\sigma_{\sigma_8} = 0.0059$ (0.7%). Comparing to the results from DES and SPT (Costanzi et al. 2021), our constraints on Ω_m and σ_8 are improved by 3 and 6 times, respectively. The improvement of constraint on the dark energy equation of state is expected to be in the same order. Here we should note that we assume a perfect mass-richness relation, that the uncertainties from redshift measurement is ignored since galaxy spec- z can be measured in the CSST spectroscopic survey. Besides, other system-

atics, such as cluster miscentering, cluster projections, and cluster triaxiality (Simet et al. 2017; Sunayama et al. 2020; Zhang et al. 2022; Wu et al. 2022), are also neglected in our analysis. In addition, we know that the abundance of galaxy clusters and the clustering of galaxies are not independent cosmological probes, since galaxy clusters represent the high peaks of galaxy density field. Our current forecast ignores their correlations, and may result in a relatively optimistic estimation. In the future work, we will study these effects in detail.

In Fig. 4, we can see that the degeneracy directions of the cosmological parameters are different for the different three probes. Hence,

Table 3. The 1σ errors of cosmological parameters and the ratios of 1σ errors to their fiducial values (relative accuracy) for the CSST 3×2pt, Spectroscopic galaxy clustering, cluster number counts, and joint surveys.

Parameter	fiducial value	3×2pt analysis		spec-z galaxy clustering		cluster number counts		joint constraint	
		1σ error	relative accuracy	1σ error	relative accuracy	1σ error	relative accuracy	1σ error	relative accuracy
Ω_m	0.314	0.01	3%	0.032	10%	0.017	5%	0.004	1%
Ω_b	0.0494	0.0028	6%	0.0073	15%	0.04	80%	0.0014	2%
w_0	-1	0.08	8%	0.2	20%	0.13	13%	0.045	4.5%
w_a	0	0.27	27%	0.86	86%	0.46	46%	0.17	17%
h	0.6732	0.0199	3%	0.0143	2%	0.0344	5%	0.002	0.3%
n_s	0.966	0.006	0.6%	0.0432	4%	0.129	13%	0.0039	0.4%
σ_8	0.82	0.009	1%	0.0177	2%	0.0059	0.7%	0.0016	0.2%

**Figure 6.** The ratios of 1σ errors to the fiducial values of the cosmological parameters for the CSST 3×2pt (blue), spectroscopic galaxy clustering (orange), and cluster number counts (green) surveys, respectively.

performing a joint constraint by including the CSST 3×2pt analysis, spectroscopic galaxy clustering, and cluster number counts surveys will provide much more precise constraint results on the cosmological parameters. As shown in Fig. 5, the 1σ errors from the joint constraint for w_0 , w_a , Ω_m and σ_8 are given by $\sigma_{w_0} = 0.045$ (4.5%), $\sigma_{w_a} = 0.17$ (17%), $\sigma_{\Omega_m} = 0.004$ (1%) and $\sigma_{\sigma_8} = 0.0016$ (0.2%). We can see that the joint constraint results are significantly improved by factors of 2-5 compared to the results from the three single CSST cosmological probes.

Besides the cosmological parameters, we also show the ratios of 1σ errors to fiducial values of the systematical parameters in the three CSST cosmological probes in Fig. 7 and Fig. 8. In Fig. 7, we can see that the constraints on photo- z bias and scatter parameters δ_z^i and σ_{z0} are smaller than $\sim 0.3\%$ and 6% , respectively, galaxy bias parameters b_i are less than $\sim 0.7\%$, and most of the multiplicative shear bias are less than $\sim 2\%$. The intrinsic alignment parameters A_{IA} and α_{IA} can be constrained within $\sim 4\%$ and 8% accuracies, respectively. We also present the ratios of the 1σ errors to the fiducial values for the five galaxy biases in the CSST spectroscopic survey in Fig. 8, and we find the constraint accuracy can be less than $\sim 3\%$. These constraint results of the galaxy biases are derived from the constraints on the redshift-dependent parameters (see Subsection 5.2). The contour maps of the systematical parameters for the 3×2pt analysis and spectroscopic galaxy clustering survey can be found in the Appendix. These results indicate that the CSST photometric and spectroscopic cosmological surveys can simultaneously put strong constraints on both cosmological and systematical parameters.

7 SUMMARY AND DISCUSSION

In the next few years, several space- and ground-based telescopes will be performed and put into service. As one of them with a wide field of view and powerful observational capability, CSST will become an excellent instrument for the cosmological probes. In this paper, we explore the CSST photometric and spectroscopic multi-probe cosmological surveys, including the 3×2pt analysis, spectroscopic galaxy clustering, and galaxy cluster number counts.

We firstly simulate the mock data of the CSST photometric surveys, including weak lensing, photometric 2D galaxy clustering, and galaxy-galaxy lensing surveys, i.e. 3×2pt analysis. The systematical effects from intrinsic alignment, photo- z calibration, galaxy bias, multiplicative error in the shear calibration, and instrument are also considered. The photo- z range is divided into 10 tomographic bins to extract more information. Secondly, we generate mock catalog and galaxy redshift distribution of the CSST spectroscopic galaxy clustering survey based on the zCOSMOS survey. The systematics from galaxy bias and instrument are included in the analysis. The spec- z range is divided into 5 bins to investigate the redshift evolution of related cosmological parameters, such as the equation of state of dark energy. Thirdly, the CSST number counts of galaxy clusters are explored. The mock data and cluster redshift distribution are created based on the halo mass function, and the redshift range is restricted within $z = 1.5$ to effectively include both CSST photometric and spectroscopic observations. The cluster redshift distribution is divided into 10 bins to explore the evolution effects.

The Fisher matrix is employed to analyze and predict the constraints on the cosmological and systematical parameters. We find that all of the three CSST cosmological probes can provide much more stringent constraints on both of cosmological and systematical parameters, that can be improved by several times at least compared to the current corresponding surveys. This is mainly due to the larger survey area, deeper magnitude limit, wider wavelength coverage, and higher imaging quality of the CSST surveys. After combining all data sets to perform the joint constraints, we find that the results can be further significantly improved, which can achieve the constraint accuracies of Ω_m and σ_8 less than 1%, and w_0 and w_a less than 5% and 20%, respectively. The systematical parameters also can be simultaneously constrained within 1%-10% accuracy. These results indicate that CSST could be a powerful telescope to explore our Universe, and would greatly improve the studies on important cosmological problems.

Comparing CSST to other next-generation survey telescopes, such as Euclid and LSST, they have similar scientific goals in cosmology and good complementarities and synergies on performances. All of them will launch or operate around 2023-2024, and measure weak gravitational lensing and galaxy clustering to study dark energy and

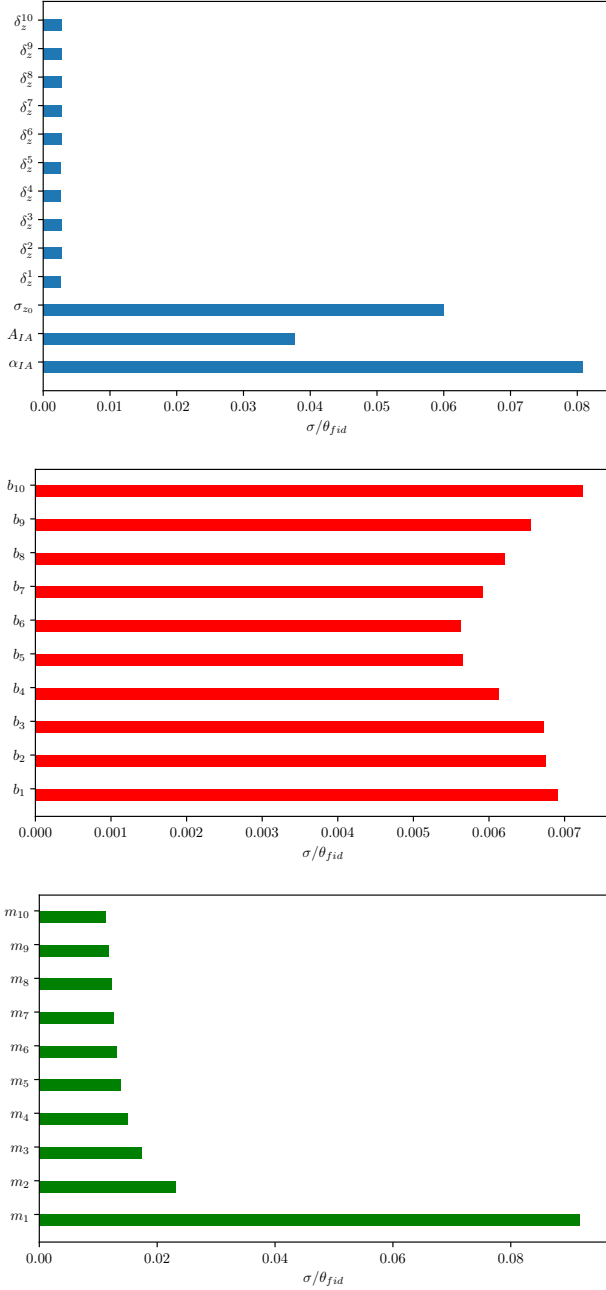


Figure 7. The ratios of 1σ errors to the fiducial values of the systematical parameters for the CSST 3×2 pt analysis.

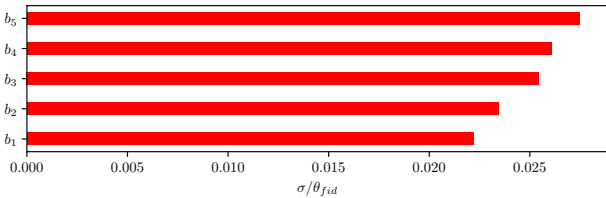


Figure 8. The ratios of 1σ errors to the fiducial values of the galaxy biases in the five spec- z bins for the CSST spectroscopic galaxy clustering survey.

dark matter. Euclid space telescope will observe 15000 deg^2 , which has large overlapping sky area covered by CSST. Since Euclid only has one single optical broadband covering 550-900 nm, it cannot accurately measure photo- z . Then CSST will be very helpful to provide accurate photo- z information with its seven photometric bands from NUV to NIR for Euclid (Cao et al. 2018; Zhou et al. 2021, 2022). On the other hand, Euclid has three near-infrared bands from 920-2000 nm, i.e. Y , J , and H , which can significantly improve the accuracy of photo- z and shear measurements in CSST surveys (Cao et al. 2018; Liu et al. 2022). As a ground-based telescope, LSST will explore 18000 deg^2 with deeper magnitude limit compared to CSST and Euclid, that can obtain more faint and high- z galaxy samples for cosmological studies. Besides, a few hundred thousand Type Ia supernovae (SNe Ia) probably can be detected by LSST per year. This would be a great complement to the study of cosmic expansion history in CSST and Euclid surveys, that only a few thousand SNe Ia are expected to be measured in their mission durations. On the other hand, CSST and Euclid have much better spatial resolution, and can measure smaller galaxies and obtain better galaxy shape measurement in weak gravitational lensing survey compared to LSST. Hence, there are large complementarities between CSST and other future survey telescopes. Synergies of these experiments can provide extremely accurate constraint on cosmological parameters, and are powerful to reveal the nature of dark energy and dark matter.

ACKNOWLEDGEMENTS

H.T.M. and Y.G. acknowledge the supports from 2020SKA0110402, MOST-2018YFE0120800, NSFC-11822305, NSFC-11773031, and NSFC-11633004. X.L.C. acknowledges the support of the National Natural Science Foundation of China through grant Nos. 11473044 and 11973047, and the Chinese Academy of Science grants QYZDJ-SSW-SLH017, XDB 23040100, and XDA15020200. Z.Q.H acknowledges the support of the National key R&D Program of China (Grant No. 2020YFC2201600), National SKA Program of China No. 2020SKA0110402, National Natural Science Foundation of China (NSFC) under Grant No. 12073088, and Guangdong Major Project of Basic and Applied Basic Research (Grant No. 2019B030302001). X.D.L acknowledges the support from the NSFC grant (No. 11803094) and the Science and Technology Program of Guangzhou, China (No. 202002030360). This work is also supported by science research grants from the China Manned Space Project with grants Nos. CMS-CSST-2021-B01 and CMS-CSST-2021-A01.

DATA AVAILABILITY

The data that support the findings of this study are available from the corresponding author, upon reasonable request.

REFERENCES

- Abbott T. M. C., et al., 2018, *Phys. Rev. D*, **98**, 043526
- Abbott T. M. C., et al., 2022a, *Phys. Rev. D*, **105**, 023520
- Abbott T. M. C., et al., 2022b, *Phys. Rev. D*, **105**, 043512
- Abdullah M. H., Klypin A., Wilson G., 2020, *ApJ*, **901**, 90
- Akeson R., et al., 2019, arXiv e-prints, p. arXiv:1902.05569
- Alam S., et al., 2021, *Phys. Rev. D*, **103**, 083533
- Albrecht A., et al., 2006, arXiv e-prints, pp astro-ph/0609591
- Alcock C., Paczynski B., 1979, *Nature*, **281**, 358
- Allen S. W., Evrard A. E., Mantz A. B., 2011, *ARA&A*, **49**, 409

- Amendola L., et al., 2013, *Living Reviews in Relativity*, **16**, 6
- Amendola L., et al., 2018, *Living Reviews in Relativity*, **21**, 2
- Amon A., et al., 2022, *Phys. Rev. D*, **105**, 023514
- Asorey J., Crocce M., Gaztañaga E., Lewis A., 2012, *MNRAS*, **427**, 1891
- Baldauf T., Smith R. E., Seljak U., Mandelbaum R., 2010, *Phys. Rev. D*, **81**, 063531
- Bellagamba F., Roncarelli M., Maturi M., Moscardini L., 2018, *MNRAS*, **473**, 5221
- Bellagamba F., et al., 2019, *MNRAS*, **484**, 1598
- Benjamin J., van Waerbeke L., Ménard B., Kilbinger M., 2010, *MNRAS*, **408**, 1168
- Bernstein G. M., 2009, *ApJ*, **695**, 652
- Beutler F., et al., 2011, *MNRAS*, **416**, 3017
- Beutler F., et al., 2017a, *MNRAS*, **464**, 3409
- Beutler F., et al., 2017b, *MNRAS*, **466**, 2242
- Blazek J., McQuinn M., Seljak U., 2011, *J. Cosmology Astropart. Phys.*, **2011**, 010
- Blazek J. A., MacCrann N., Troxel M. A., Fang X., 2019, *Phys. Rev. D*, **100**, 103506
- Bridle S., King L., 2007, *New Journal of Physics*, **9**, 444
- Brieden S., Gil-Marín H., Verde L., 2021, *J. Cosmology Astropart. Phys.*, **2021**, 054
- Bullock J. S., Boylan-Kolchin M., 2017, *ARA&A*, **55**, 343
- Cao Y., et al., 2018, *MNRAS*, **480**, 2178
- Carron J., 2013, *A&A*, **551**, A88
- Chevallier M., Polarski D., 2001, *International Journal of Modern Physics D*, **10**, 213
- Chisari N. E., et al., 2019, *ApJS*, **242**, 2
- Clampitt J., et al., 2017, *MNRAS*, **465**, 4204
- Cole S., et al., 2005, *MNRAS*, **362**, 505
- Copeland D., Taylor A., Hall A., 2018, *MNRAS*, **480**, 2247
- Costanzi M., et al., 2019, *MNRAS*, **488**, 4779
- Costanzi M., et al., 2021, *Phys. Rev. D*, **103**, 043522
- Das S., Errard J., Spergel D., 2013, arXiv e-prints, p. arXiv:1311.2338
- Dawson K. S., et al., 2013, *AJ*, **145**, 10
- Dawson K. S., et al., 2016, *AJ*, **151**, 44
- Di Valentino E., et al., 2021, *Astroparticle Physics*, **131**, 102605
- Duncan C. A. J., Harnois-Déraps J., Miller L., Langedijk A., 2022, *MNRAS*, **515**, 1130
- Eifler T., et al., 2021a, *MNRAS*, **507**, 1514
- Eifler T., et al., 2021b, *MNRAS*, **507**, 1746
- Eisenstein D. J., et al., 2011, *AJ*, **142**, 72
- Elvin-Poole J., et al., 2018, *Phys. Rev. D*, **98**, 042006
- Euclid Collaboration et al., 2020, *A&A*, **642**, A191
- Euclid Collaboration et al., 2022, *A&A*, **662**, A93
- Fenech Conti I., Herbonnet R., Hoekstra H., Merten J., Miller L., Viola M., 2017, *MNRAS*, **467**, 1627
- Font-Ribera A., McDonald P., Mostek N., Reid B. A., Seo H.-J., Slosar A., 2014, *J. Cosmology Astropart. Phys.*, **2014**, 023
- Forozaan S., Krolewski A., Percival W. J., 2021, *J. Cosmology Astropart. Phys.*, **2021**, 044
- Fumagalli A., et al., 2021, *A&A*, **652**, A21
- Giblin B., et al., 2021, *A&A*, **645**, A105
- Gil-Marín H., et al., 2016a, *MNRAS*, **460**, 4188
- Gil-Marín H., et al., 2016b, *MNRAS*, **460**, 4210
- Gil-Marín H., Percival W. J., Verde L., Brownstein J. R., Chuang C.-H., Kitaura F.-S., Rodríguez-Torres S. A., Olmstead M. D., 2017, *MNRAS*, **465**, 1757
- Gil-Marín H., et al., 2020, *MNRAS*, **498**, 2492
- Gillis B. R., Taylor A. N., 2019, *MNRAS*, **482**, 402
- Gong Y., et al., 2019, *ApJ*, **883**, 203
- Haiman Z., Mohr J. J., Holder G. P., 2001, *ApJ*, **553**, 545
- Hamilton A. J. S., 1998, in Hamilton D., ed., *Astrophysics and Space Science Library Vol. 231, The Evolving Universe*. p. 185 (arXiv:astro-ph/9708102), doi:10.1007/978-94-011-4960-0_17
- Hasan I. S., Schmidt S. J., Schneider M. D., Tyson J. A., 2022, *MNRAS*, **511**, 1029
- Heneka C., Rapetti D., Cataneo M., Mantz A. B., Allen S. W., von der Linden A., 2018, *MNRAS*, **473**, 3882
- Heymans C., et al., 2006, *MNRAS*, **368**, 1323
- Heymans C., et al., 2013, *MNRAS*, **432**, 2433
- Heymans C., et al., 2021, *A&A*, **646**, A140
- Hikage C., et al., 2019, *PASJ*, **71**, 43
- Hildebrandt H., et al., 2017, *MNRAS*, **465**, 1454
- Hildebrandt H., et al., 2021, *A&A*, **647**, A124
- Hinshaw G., et al., 2013, *ApJS*, **208**, 19
- Hirata C. M., Seljak U., 2004, *Phys. Rev. D*, **70**, 063526
- Hoekstra H., Jain B., 2008, *Annual Review of Nuclear and Particle Science*, **58**, 99
- Hou Z., et al., 2014, *ApJ*, **782**, 74
- Hu W., 1999, *ApJ*, **522**, L21
- Huang Z., Verde L., Vernizzi F., 2012, *J. Cosmology Astropart. Phys.*, **2012**, 005
- Huang H.-J., Eifler T., Mandelbaum R., Dodelson S., 2019, *MNRAS*, **488**, 1652
- Huterer D., Takada M., Bernstein G., Jain B., 2006, *MNRAS*, **366**, 101
- Ivanov M. M., Simonović M., Zaldarriaga M., 2020, *J. Cosmology Astropart. Phys.*, **2020**, 042
- Ivezić Z., et al., 2019, *ApJ*, **873**, 111
- Jain B., Jarvis M., Bernstein G., 2006, *J. Cosmology Astropart. Phys.*, **2006**, 001
- Jarvis M., et al., 2016, *MNRAS*, **460**, 2245
- Joachimi B., Bridle S. L., 2010, *A&A*, **523**, A1
- Joachimi B., et al., 2015, *Space Sci. Rev.*, **193**, 1
- Joachimi B., et al., 2021, *A&A*, **646**, A129
- Jones D. H., et al., 2009, *MNRAS*, **399**, 683
- Kaiser N., 1987, *MNRAS*, **227**, 1
- Kaiser N., Squires G., 1993, *ApJ*, **404**, 441
- Kiessling A., et al., 2015, *Space Sci. Rev.*, **193**, 67
- Kilbinger M., 2015, *Reports on Progress in Physics*, **78**, 086901
- Kirk D., Rassat A., Host O., Bridle S., 2012, *MNRAS*, **424**, 1647
- Kirk D., et al., 2015, *Space Sci. Rev.*, **193**, 139
- Koester B. P., et al., 2007, *ApJ*, **660**, 239
- Komatsu E., et al., 2011, *ApJS*, **192**, 18
- Krause E., Eifler T., 2017, *MNRAS*, **470**, 2100
- Krause E., Eifler T., Blazek J., 2016, *MNRAS*, **456**, 207
- Krause E., et al., 2017, arXiv e-prints, p. arXiv:1706.09359
- Krause E., et al., 2021, arXiv e-prints, p. arXiv:2105.13548
- Laureijs R., et al., 2011, arXiv e-prints, p. arXiv:1110.3193
- Lesci G. F., et al., 2022a, *A&A*, **659**, A88
- Lesci G. F., et al., 2022b, *A&A*, **665**, A100
- Lewis A., Challinor A., Lasenby A., 2000, *ApJ*, **538**, 473
- Li X.-D., Park C., Forero-Romero J. E., Kim J., 2014, *ApJ*, **796**, 137
- Li X.-D., et al., 2018, *ApJ*, **856**, 88
- Li X.-D., Miao H., Wang X., Zhang X., Fang F., Luo X., Huang Q.-G., Li M., 2019, *ApJ*, **875**, 92
- Lilly S. J., et al., 2009, *ApJS*, **184**, 218
- Lima M., Hu W., 2005, *Phys. Rev. D*, **72**, 043006
- Linder E. V., 2003, *Phys. Rev. Lett.*, **90**, 091301
- Liu D. Z., et al., 2022, arXiv e-prints, p. arXiv:2210.16341
- López-Corredoira M., 2014, *ApJ*, **781**, 96
- Ma Z., Hu W., Huterer D., 2006, *ApJ*, **636**, 21
- Mahony C., et al., 2022, *MNRAS*, **513**, 1210
- Mandelbaum R., 2018, *ARA&A*, **56**, 393
- Mandelbaum R., et al., 2005, *MNRAS*, **361**, 1287
- Mandelbaum R., Slosar A., Baldauf T., Seljak U., Hirata C. M., Nakajima R., Reyes R., Smith R. E., 2013, *MNRAS*, **432**, 1544
- Marinoni C., Buzzi A., 2010, *Nature*, **468**, 539
- Martinelli M., et al., 2021, *A&A*, **649**, A100
- Massey R., et al., 2013, *MNRAS*, **429**, 661
- McQuinn M., White M., 2013, *MNRAS*, **433**, 2857
- Mead A. J., Peacock J. A., Heymans C., Joudaki S., Heavens A. F., 2015, *MNRAS*, **454**, 1958
- Mead A. J., Heymans C., Lombriser L., Peacock J. A., Steele O. I., Winther H. A., 2016, *MNRAS*, **459**, 1468

- Mead A. J., Brieden S., Tröster T., Heymans C., 2021, *MNRAS*, **502**, 1401
- Munshi D., Valageas P., van Waerbeke L., Heavens A., 2008, *Phys. Rep.*, **462**, 67
- Neveux R., et al., 2020, *MNRAS*, **499**, 210
- Oguri M., 2014, *MNRAS*, **444**, 147
- Oguri M., Takada M., 2011, *Phys. Rev. D*, **83**, 023008
- Oguri M., et al., 2018, *PASJ*, **70**, S20
- Padmanabhan N., et al., 2007, *MNRAS*, **378**, 852
- Park Y., Sunayama T., Takada M., Kobayashi Y., Miyatake H., More S., Nishimichi T., Sugiyama S., 2021a, arXiv e-prints, p. arXiv:2112.09059
- Park Y., Rozo E., Krause E., 2021b, *Phys. Rev. Lett.*, **126**, 021301
- Parkinson D., et al., 2012, *Phys. Rev. D*, **86**, 103518
- Paulin-Henriksson S., Amara A., Voigt L., Refregier A., Bridle S. L., 2008, *A&A*, **484**, 67
- Percival W. J., et al., 2010, *MNRAS*, **401**, 2148
- Planck Collaboration et al., 2014, *A&A*, **571**, A16
- Planck Collaboration et al., 2020, *A&A*, **641**, A6
- Porredon A., et al., 2021, arXiv e-prints, p. arXiv:2105.13546
- Prat J., et al., 2018, *Phys. Rev. D*, **98**, 042005
- Prat J., et al., 2022, *Phys. Rev. D*, **105**, 083528
- Press W. H., Schechter P., 1974, *ApJ*, **187**, 425
- Pujol A., Sureau F., Bobin J., Courbin F., Gentile M., Kilbinger M., 2020a, *A&A*, **641**, A164
- Pujol A., Bobin J., Sureau F., Guinot A., Kilbinger M., 2020b, *A&A*, **643**, A158
- Rau M. M., Morrison C. B., Schmidt S. J., Wilson S., Mandelbaum R., Mao Y. Y., Mao Y. Y., LSST Dark Energy Science Collaboration 2022, *MNRAS*, **509**, 4886
- Rodríguez-Monroy M., et al., 2022, *MNRAS*, **511**, 2665
- Rosell A. C., et al., 2022, *MNRAS*, **509**, 778
- Rozo E., et al., 2009, *ApJ*, **703**, 601
- Rozo E., et al., 2010, *ApJ*, **708**, 645
- Rozo E., Rykoff E. S., Becker M., Reddick R. M., Wechsler R. H., 2015, *MNRAS*, **453**, 38
- Rykoff E. S., et al., 2012, *ApJ*, **746**, 178
- Rykoff E. S., et al., 2014, *ApJ*, **785**, 104
- Rykoff E. S., et al., 2016, *ApJS*, **224**, 1
- Salvati L., Douspis M., Aghanim N., 2020, *A&A*, **643**, A20
- Samuroff S., et al., 2019, *MNRAS*, **489**, 5453
- Sartoris B., et al., 2016, *MNRAS*, **459**, 1764
- Schaan E., Krause E., Eifler T., Doré O., Miyatake H., Rhodes J., Spergel D. N., 2017, *Phys. Rev. D*, **95**, 123512
- Schaan E., Ferraro S., Seljak U., 2020, *J. Cosmology Astropart. Phys.*, **2020**, 001
- Schneider A., Teyssier R., Stadel J., Chisari N. E., Le Brun A. M. C., Amara A., Refregier A., 2019, *J. Cosmology Astropart. Phys.*, **2019**, 020
- Secco L. F., et al., 2022, *Phys. Rev. D*, **105**, 023515
- Seo H.-J., Eisenstein D. J., 2007, *ApJ*, **665**, 14
- Sheth R. K., Tormen G., 1999, *MNRAS*, **308**, 119
- Sievers J. L., et al., 2013, *J. Cosmology Astropart. Phys.*, **2013**, 060
- Simet M., McClintock T., Mandelbaum R., Rozo E., Rykoff E., Sheldon E., Wechsler R. H., 2017, *MNRAS*, **466**, 3103
- Singh S., Mandelbaum R., Seljak U., Slosar A., Vazquez Gonzalez J., 2017, *MNRAS*, **471**, 3827
- Stölzner B., Joachimi B., Korn A., Hildebrandt H., Wright A. H., 2021, *A&A*, **650**, A148
- Sunayama T., et al., 2020, *MNRAS*, **496**, 4468
- Sunyaev R. A., Zeldovich Y. B., 1972, Comments on Astrophysics and Space Physics, **4**, 173
- Takahashi R., Sato M., Nishimichi T., Taruya A., Oguri M., 2012, *ApJ*, **761**, 152
- Tanoglidis D., Chang C., Frieman J., 2020, *MNRAS*, **491**, 3535
- Taylor A. N., Kitching T. D., 2018, *MNRAS*, **477**, 3397
- Taylor P. L., Kitching T. D., McEwen J. D., 2018, *Phys. Rev. D*, **98**, 043532
- Tegmark M., 1997, *Phys. Rev. Lett.*, **79**, 3806
- Tegmark M., Taylor A. N., Heavens A. F., 1997, *ApJ*, **480**, 22
- Tegmark M., et al., 2002, *ApJ*, **571**, 191
- Thiele L., Duncan C. A. J., Alonso D., 2020, *MNRAS*, **491**, 1746
- Tinker J., Kravtsov A. V., Klypin A., Abazajian K., Warren M., Yepes G., Gottlöber S., Holz D. E., 2008, *ApJ*, **688**, 709
- To C., et al., 2021a, *Phys. Rev. Lett.*, **126**, 141301
- To C.-H., et al., 2021b, *MNRAS*, **502**, 4093
- Tröster T., et al., 2021, *A&A*, **649**, A88
- Troxel M. A., Ishak M., 2015, *Phys. Rep.*, **558**, 1
- Troxel M. A., et al., 2018, *Phys. Rev. D*, **98**, 043528
- Tutusaus I., et al., 2020, *A&A*, **643**, A70
- Unruh S., Schneider P., Hilbert S., Simon P., Martin S., Puertas J. C., 2020, *A&A*, **638**, A96
- Vallinotto A., 2012, *ApJ*, **759**, 32
- Verde L., Treu T., Riess A. G., 2019, *Nature Astronomy*, **3**, 891
- Wang Y., Chuang C.-H., Hirata C. M., 2013, *MNRAS*, **430**, 2446
- Weaverdyck N., Huterer D., 2021, *MNRAS*, **503**, 5061
- Wu H.-Y., et al., 2022, *MNRAS*, **515**, 4471
- Yoo J., Seljak U., 2012, *Phys. Rev. D*, **86**, 083504
- Zhan H., 2006, *J. Cosmology Astropart. Phys.*, **2006**, 008
- Zhan H., 2011, *Scientia Sinica Physica, Mechanica & Astronomica*, **41**, 1441
- Zhan H., 2018, in 42nd COSPAR Scientific Assembly. pp E1.16–4–18
- Zhan H., 2021, *Chinese Science Bulletin*, **66**, 1290
- Zhan H., Knox L., 2006, *ApJ*, **644**, 663
- Zhan H., Knox L., Tyson J. A., 2009, *ApJ*, **690**, 923
- Zhang P., Pen U.-L., Bernstein G., 2010, *MNRAS*, **405**, 359
- Zhang Z., et al., 2022, arXiv e-prints, p. arXiv:2202.08211
- Zhou X., et al., 2021, *ApJ*, **909**, 53
- Zhou X., et al., 2022, *MNRAS*, **512**, 4593
- Zuntz J., et al., 2015, *Astronomy and Computing*, **12**, 45
- Zuntz J., et al., 2021, *The Open Journal of Astrophysics*, **4**, 13
- d’Amico G., Gleyzes J., Kokron N., Markovic K., Senatore L., Zhang P., Beutler F., Gil-Marín H., 2020, *J. Cosmology Astropart. Phys.*, **2020**, 005
- de Haan T., et al., 2016, *ApJ*, **832**, 95
- van Uitert E., et al., 2018, *MNRAS*, **476**, 4662

APPENDIX A: CONTOUR MAPS OF THE SYSTEMATICAL PARAMETERS

The contour maps of the systematical parameters in the CSST $3 \times 2pt$ probes, i.e. IA and photo- z calibration, galaxy bias, and multiplicative error, are shown in Fig. A1, A2, and A3, respectively. The constraint results of the galaxy biases in the CSST spectroscopic galaxy clustering survey are also presented in Fig. A4.

This paper has been typeset from a \LaTeX file prepared by the author.

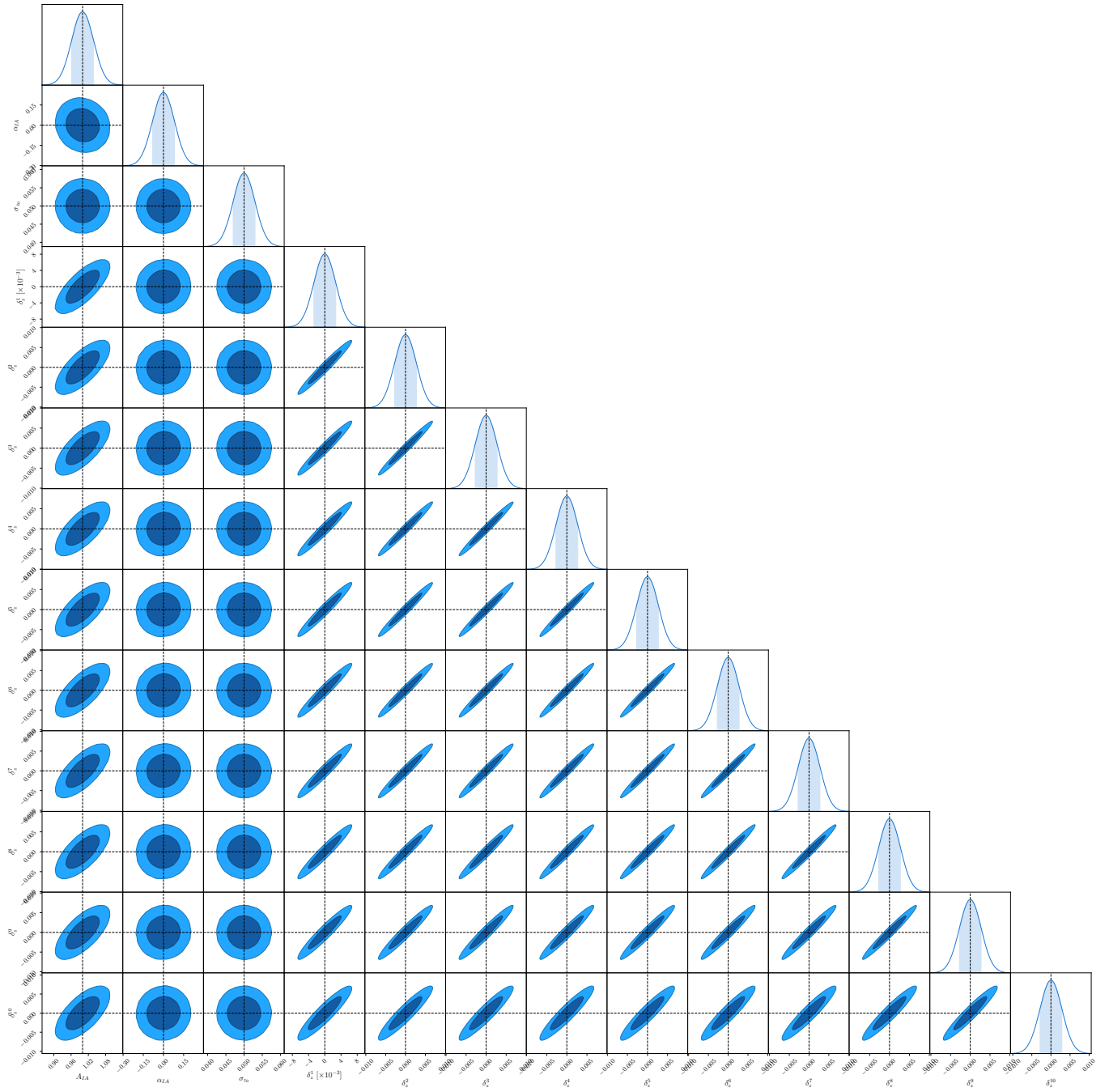


Figure A1. Constraint results of the parameters for the IA and photo- z calibration in the CSST 3 \times 2pt probes.

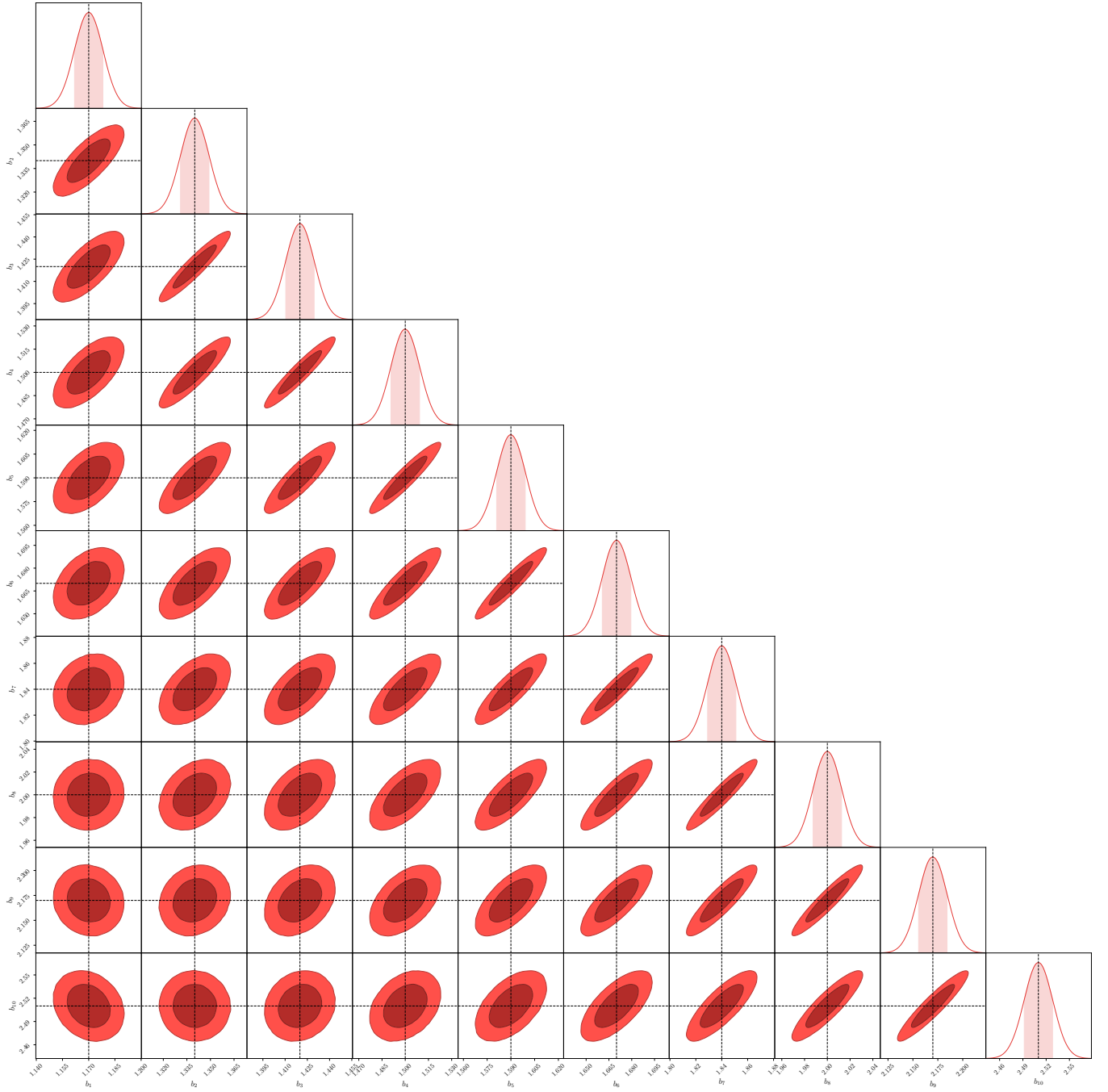


Figure A2. Constraint results of the galaxy biases in the 10 photo- z bins of the CSST 3 \times 2pt probes.

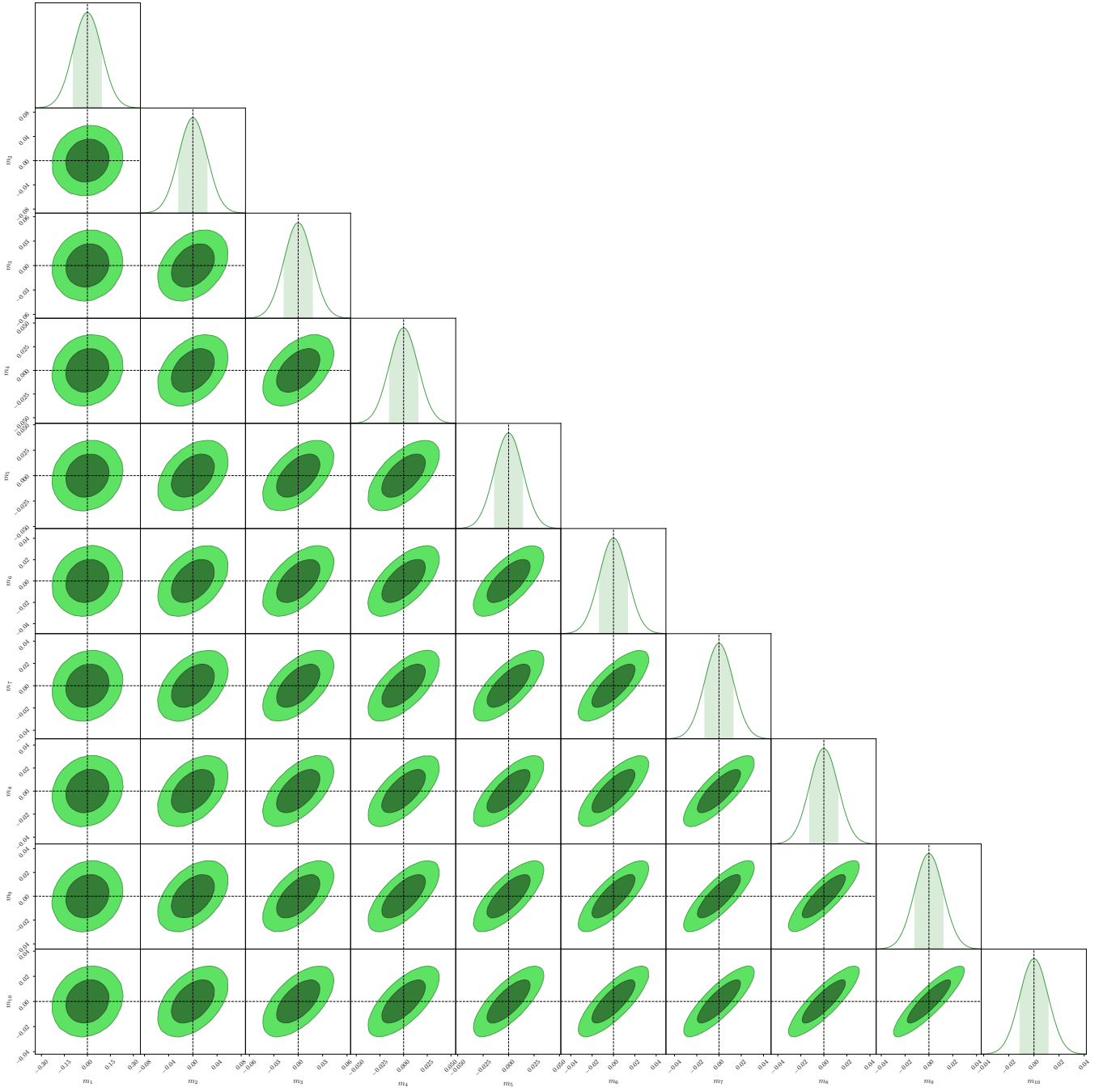


Figure A3. Constraint results of the shear multiplicative biases in the 10 photo- z bins of the CSST 3 \times 2pt probes.

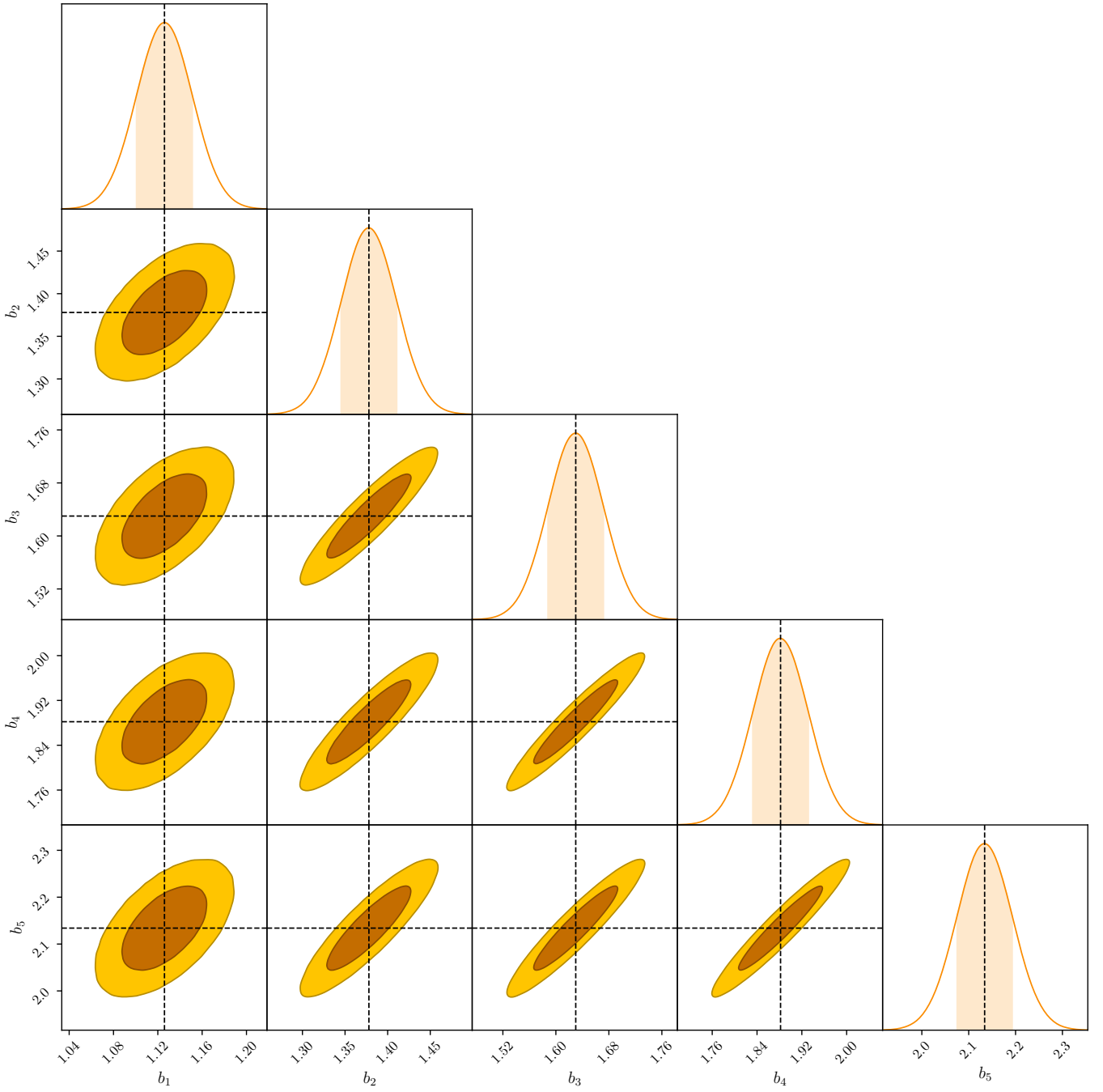


Figure A4. Constraint results of the galaxy biases in the 5 spec- z bins of the CSST spectroscopic galaxy clustering survey.